PHYSICAL REVIEW VOLUME 163, NUMBER 3 15 NOVEMBER 1967

Spectroscopic Investigation of Group-III Acceptor States in Silicon[*]

A. Onton,[†] P. Fisher, and A. K. Ramdas
Department of Physics, Purdue University, Lafayette, Indiana

(Received 26 June 1967)

The excitation spectra associated with the group-III acceptor impurities; boron, aluminum, gallium, and indium in silicon, have been studied at low temperatures using grating spectrometers. The behavior of these spectra under uniaxial stress has been studied employing polarized radiation. The improved resolution of the present investigation has revealed details not reported previously for the zero-stress spectra. The line reported by earlier workers at 68.26 meV for gallium impurity has been resolved into three components at 67.95, 68.25, and 68.43 meV. For aluminum and indium impurity, the lines at 64.99 and 150.88 meV, respectively, have each been resolved into two components, at 64.96 and 65.16 meV and at 150.80 and 151.08 meV, respectively. The presence of the shoulder at 39.91 meV on the excitation line of boron at 39.64 meV has been confirmed. Also, transitions from the ground state associated with the $p_{3/2}$ valence band to excited states associated with the split-off $p_{1/2}$ valence band have been observed for gallium and indium impurity, in addition to those of boron and aluminum reported previously. It has been established that the ground state has Γ_8 symmetry for all the impurities studied. The first three excited states participating in the optical transitions (corresponding to lines 1–3) also have Γ_8 symmetry. The behavior of the line-4 complex under stress is consistent with the final states being $\Gamma_6+\Gamma_7+\Gamma_8$. The stress-induced sublevels of the Γ_8 final states of lines 1 and 2 have opposite ordering for compression along $\langle 111\rangle$. The various states of a given impurity differ in their quantitative response to stress. Also, there are marked differences in the quantitative stress behavior of these states from impurity to impurity.

I. INTRODUCTION

A STUDY of the excitation spectrum associated with the localized states of an impurity in a semiconductor yields significant information about both the impurity and the host material. The first such observations were made by Burstein *et al.*,[1] who examined the spectrum of boron in silicon. Since then the group-III impurities, boron, aluminum, gallium, and indium in silicon have been studied by several workers.[2–16] It is well known that the valence band of silicon exhibits spin-orbit splitting, the $p_{1/2}$ valence band lying below the $p_{3/2}$ valence band. Optical transitions from the $p_{3/2}$ impurity ground state to excited states associated with *both* valence bands have been observed.[8]

In recent years the use of uniaxial stress in the study of optical spectra, i.e., the piezospectroscopic effect,[17] has proved to be extremely fruitful in the understanding of energy states of donors and acceptors in silicon and germanium. The stress effects for group-V donors in silicon and germanium have been studied by Aggarwal and Ramdas[18] and by Reuszer and Fisher,[19] respectively. Other donor systems studied from this point of view are lithium in silicon,[20] donorlike irradiation-induced defects in silicon,[21] donorlike heat-treatment centers in silicon,[22] sulfur donors in silicon,[23] and selenium[24] and tellurium[25] donors in the III-V compound, aluminum antimonide. The first application of the piezospectroscopic technique to the study of acceptor states was made by Jones and Fisher; they have studied neutral zinc[26] and the group-

---

[*] Work supported in part by the U. S. Army Research Office, Durham, U. S. Office of Naval Research, and the Advanced Research Projects Agency.

[†] Present Address: IBM Watson Research Center, Yorktown Heights, New York.

[1] E. Burstein, J. J. Oberly, J. W. Davisson, and B. W. Henvis, Phys. Rev. **82**, 764 (1951).

[2] E. Burstein, E. E. Bell, J. W. Davisson, and M. Lax, J. Phys. Chem. **57**, 849 (1953).

[3] E. Burstein, G. Picus, B. Henvis, and M. Lax, Phys. Rev. **98**, 1536 (1955).

[4] R. Newman, Phys. Rev. **99**, 465 (1955).

[5] E. Burstein, G. Picus, and N. Sclar, in *Photoconductivity Conference*, edited by R. G. Breckenridge, B. R. Russell, and E. E. Hahn (John Wiley & Sons, Inc., New York, 1956), p. 353.

[6] R. Newman, Phys. Rev. **103**, 103 (1956).

[7] H. J. Hrostowski and R. H. Kaiser, J. Phys. Chem. Solids **4**, 148 (1958).

[8] S. Zwerdling, K. J. Button, B. Lax, and L. M. Roth, Phys. Rev. Letters **4**, 173 (1960).

[9] S. Zwerdling, K. J. Button, and B. Lax, Phys. Rev. **118**, 975 (1960).

[10] K. Colbow, J. W. Bichard, and J. C. Giles, Can. J. Phys. **40**, 1436 (1962).

[11] K. Colbow, Can. J. Phys. **41**, 1801 (1963).

[12] P. Fisher and A. K. Ramdas, Phys. Letters **16**, 26 (1965).

[13] M. W. Skoczylas and J. J. White, Can. J. Phys. **43**, 1388 (1965).

[14] A. Onton and A. K. Ramdas, Bull. Am. Phys. Soc. **11**, 51 (1966).

[15] A. Onton, P. Fisher, and A. K. Ramdas, Bull. Am. Phys. Soc. **11**, 740 (1966).

[16] P. Fisher, R. L. Jones, A. Onton, and A. K. Ramdas, J. Phys. Soc. Japan Suppl. **21**, 224 (1966).

[17] This term has been coined by A. A. Kaplyanskii, who has made extensive contributions to the study of optical spectra under stress. See, for example, the review article by P. P. Feofilov and A. A. Kaplyanskii, Usp. Fiz. Nauk **76**, 201 (1962) [English transl.: Soviet Phys.—Usp. **5**, 79 (1962).]

[18] R. L. Aggarwal and A. K. Ramdas, Phys. Rev. **137**, A602 (1965).

[19] J. H. Reuszer and P. Fisher, Phys. Rev. **140**, A245 (1965).

[20] R. L. Aggarwal, P. Fisher, V. Mourzine, and A. K. Ramdas, Phys. Rev. **138**, A882 (1965).

[21] M. G. Rao and A. K. Ramdas, Bull. Am. Phys. Soc. **10**, 123 (1965).

[22] R. L. Aggarwal and A. K. Ramdas, Bull. Am. Phys. Soc. **9**, 61 (1964).

[23] W. E. Krag, W. H. Kleiner, H. J. Zeiger, and S. Fischler, J. Phys. Soc. Japan Suppl. **21**, 230 (1966).

[24] B. T. Ahlburn and A. K. Ramdas, Bull. Am. Phys. Soc. **12**, 139 (1967).

[25] B. T. Ahlburn and A. K. Ramdas (unpublished results).

[26] R. L. Jones and P. Fisher, Bull. Am. Phys. Soc. **9**, 237 (1964); see also Ref. 16.

III acceptor thallium[27] in germanium. Recently, Dickey and Dimmock[28] have reported the results of a piezospectroscopic investigation of the group-III acceptors gallium, indium, and thallium in germanium. Barra and Fisher[29] have recently initiated such a study for singly ionized zinc in germanium. The first study of such effects for acceptors in silicon is that of Fisher and Ramdas,[12] who studied the spectrum of boron in silicon under uniaxial stress; Skoczylas and White[13] also independently reported the results of a similar study for the same impurity in silicon, without, however, employing polarized radiation. Stress effects for the $p_{1/2}$ spectra of group-III acceptors in silicon were first reported by Onton and Ramdas.[14] A brief account of some of these results appear in a paper by Fisher *et al.*[16]

The purpose of the present investigation is a comprehensive study of the excitation spectra of boron, aluminum, gallium, and indium in silicon, including both the $p_{1/2}$ and $p_{3/2}$ series, with and without uniaxial stress.

II. EXPERIMENTAL PROCEDURE

The optical samples were cut from single crystal ingots[30] of silicon doped with boron, aluminum, gallium, or indium. The room-temperature carrier concentrations were in the range 10^{15}–2×10^{16} cm^{-3} for the samples used in the present measurements. The crystallographic orientation of the samples was determined by x rays or by the optical method described by Hancock and Edelman.[31] In the present studies, uniaxial compression was applied along the $\langle100\rangle$, $\langle111\rangle$, or $\langle110\rangle$ direction.

A single-beam, double-pass Perkin-Elmer grating monochromator, Model 99-G, equipped with Bausch & Lomb, plane, reflection, blazed gratings and appropriate optical filtering systems, was used for the measurements, except for those of Figs. 12–14, for which a Perkin-Elmer 210 monochromator was used. The radiation was polarized by passing it through a Perkin-Elmer wire-grid polarizer with AgCl substrate[32] for wavelengths below $\sim20\,\mu$, and a "pile-of-plates" polyethylene polarizer,[33] for wavelengths above $\sim17\,\mu$. The optical cryostat used in the transmission measurements is described elsewhere.[34] In all the measurements, the samples were clamped to a copper cold finger which in turn was in contact with liquid helium. A Reeder thermocouple[35] was used as detector.

The uniaxial compression was produced by following a technique similar to that described by Rose-Innes.[36] In this technique, the silicon sample is constrained in a copper jig, and the whole assembly attached to the copper tail of the cryostat. During the process of cooling from room temperature to liquid-helium temperature, copper contracts more than silicon. This differential contraction is uniaxial in view of the geometry of the copper jig and the silicon sample. Using the relative change in length with temperature reported in the literature for silicon[37] and copper,[38] a maximum strain of about 10^{-3} can be expected. During cooling, the grease freezes to form a solid bond between the end of the sample and the jig. A certain amount of yield occurs before the grease bond becomes solid, and thus strains $<10^{-3}$ were obtained. With this technique it was possible to strain samples of a wide range of cross sections, viz., ~2 to 20 mm^2.

The data were processed with the aid of a program written for an IBM 7094 computer. The data were recorded for this purpose in the following manner.[39] The amplified detector output was punched out on command on an IBM 026 key punch. The number punched out, an integer from 000 to 999, was derived from the angular position of the tap of the potentiometer of a Leeds and Northrup Speedomax recorder. The potentiometer shaft position was sensed by a Datex encoder Model C-111,[40] the encoder output being stored by a Datex K-101 Control Chassis,[40] which also provided a digital decimal output in the form of contact closures. This output was transmitted to the keypunch by a time-serializer designed and built in this laboratory.[41] The amplified detector output was recorded at regular intervals at command of a "pick-off" unit geared to the wavelength drive of the monochromator. The computer output could be obtained in the form of a plot prepared by a Calcomp Model 563 digital incremental plotter.

III. THEORY

A. Zero Stress

The top of the valence band of silicon is known to be at $\mathbf{k}=0$,[42] the wave functions in the tight-binding

---

[27] R. L. Jones and P. Fisher, Solid State Commun. **2**, 369 (1964).

[28] D. H. Dickey and J. O. Dimmock, J. Phys. Chem. Solids **28**, 529 (1967).

[29] F. Barra and P. Fisher, Bull. Am. Phys. Soc. **12**, 658 (1967).

[30] Material Si(Al)10 was purchased from Allegheny Electronic Chemicals Co., Bradford, Pa.; Si(B) #288 was grown at Purdue University by P. H. Klose; all other material was obtained from Texas Instruments, Inc., Dallas, Texas.

[31] R. D. Hancock and S. Edelman, Rev. Sci. Instr. **27**, 1082 (1956); J. W. Edwards, Semicond. Proc. **6**, 30 (1963); *ibid.* **6**, 34 (1963).

[32] G. R. Bird and M. Parrish, Jr., J. Opt. Soc. Am. **50**, 886 (1960).

[33] A. Mitsuishi, Y. Yamada, S. Fujita, and H. Yoshinaga, J. Opt. Soc. Am. **50**, 433 (1960).

[34] P. Fisher, W. H. Haak, E. J. Johnson, and A. K. Ramdas, *Proceedings of the Eighth Symposium on the Art of Glassblowing* (The American Scientific Glassblowing Society, Wilmington, Delaware, 1963), p. 136.

[35] Manufactured by Charles M. Reeder and Co., Inc., 196 Victor Avenue, Detroit 3, Michigan.

[36] A. C. Rose-Innes, Proc. Phys. Soc. (London) **72**, 514 (1958).

[37] D. F. Gibbons, Phys. Rev. **112**, 136 (1958).

[38] D. Bijl and H. Pullan, Physica **21**, 285 (1955).

[39] For a detailed description of the automation and processing of data, see A. Onton, Ph.D. thesis, Purdue University, 1967 (unpublished).

[40] These items were purchased from Lectronic Research Laboratories, Inc., 715 Arch Street, Philadelphia 6, Pa.

[41] The authors would like to thank Dr. H. P. Larson and Dr. K. L. Andrew for advice on the design of the time serializer.

[42] H. Brooks, in *Advances in Electronics and Electron Physics*, edited by L. Marton (Academic Press Inc., New York, 1955), Vol. VII, p. 85.

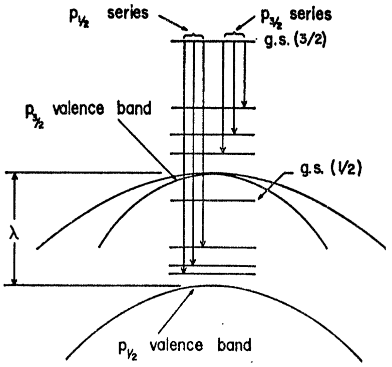

FIG. 1. The spin-orbit split valence band of silicon with associated acceptor states. Here g.s. is the ground state; λ is the spin-orbit splitting at $\mathbf{k}=0$.

approximation being constructed from $3p$ atomic orbitals.[43] When spin-orbit interaction is included, the valence band edge splits into a fourfold and a twofold degenerate band as shown in Fig. 1. These two maxima are characterized by the atomic $J=\frac{3}{2}$ and $J=\frac{1}{2}$ total angular momentum quantum numbers, respectively; the wave functions of these states form bases for the irreducible representations Γ_8^+ and Γ_7^+, respectively, of the double point group $\bar{O}_h$ (see Ref. 43).

The substitutional group-III acceptors in silicon have been treated in the framework of the effective-mass theory.[44,45] The resulting effective-mass wave equations are

$$\sum_{j'=1}^{6} D_{jj'}{}^{\alpha\beta}\left(\frac{1}{i}\frac{\partial}{\partial x^\alpha}\right)\left(\frac{1}{i}\frac{\partial}{\partial x^\beta}\right)F_{j'}(\mathbf{r})-\lambda\epsilon_j F_j(\mathbf{r}) +\frac{e^2}{\kappa r}F_j(\mathbf{r})=EF_j(\mathbf{r}). \tag{1}$$

The coefficients $D_{jj'}{}^{\alpha\beta}$ are numerical constants characteristic of the material and are of the dimension $\hbar^2/m_0$; $\epsilon_j=0$ for $j=1$–4 and $\epsilon_j=1$ for $j=5$ and 6; λ is the spin-orbit splitting; κ is the dielectric constant of the material.

The total wave function of an acceptor state is given by

$$\psi(\mathbf{r})=\sum_j F_j(\mathbf{r})\phi_j(\mathbf{r}), \tag{2}$$

TABLE I. Decomposition of hydrogenic states to those of the double group $\bar{T}_d$.

$p_{3/2}$ Valence band	T	Parity	$\bar{T}_d$ decomposition
1s level	$\frac{3}{2}$	odd	Γ_8
np level	$\frac{5}{2}, \frac{3}{2}, \frac{1}{2}$	even	$\Gamma_6+\Gamma_7+2\Gamma_8$
$p_{1/2}$ Valence band			
1s level	$\frac{1}{2}$	odd	Γ_7
np level	$\frac{3}{2}, \frac{1}{2}$	even	$\Gamma_6+\Gamma_8$

where $F_j(\mathbf{r})$ are the envelope functions that are solutions of the effective-mass equations, Eq. (1). Here $\phi_j(\mathbf{r})$ are the Bloch functions at the top of the valence band with which the localized state is associated. The index j sums over the Bloch functions of the bands considered in the formation of the acceptor state. The $\psi(\mathbf{r})$ are eigenfunctions of the total angular momentum,[46,47]

$$\mathbf{T}=\mathbf{L}+\mathbf{J}, \tag{3}$$

where $\mathbf{L}$ is the angular momentum of the $F_j(\mathbf{r})$, and $\mathbf{J}$ is the angular momentum of the Bloch functions $\phi_j(\mathbf{r})$. The parity of the $\psi(\mathbf{r})$ may be determined from the parities of the $F_j(\mathbf{r})$ and $\phi_j(\mathbf{r})$; the $F_j(\mathbf{r})$ are hydrogen-like functions. In the excitation spectra, the transitions of interest are of the type $1s\rightarrow np$ with $n=2, 3, \cdots$, with even parity for the ground-state 1s-like envelope function and odd parity for the p-like envelope functions. Since the $\phi_j(\mathbf{r})$ which enter in Eq. [2] are constructed from p-type atomic orbitals,[43] they have odd parity under $\bar{T}_d$, the site symmetry of the impurity being T_d. Thus, for example, the $\psi(\mathbf{r})$ describing p-like excited states associated with the $p_{3/2}$ valence band have total angular momenta $\mathbf{T}=\frac{5}{2}, \frac{3}{2}, \frac{1}{2}$, and even parity; the irreducible representations of the full rotation group for these values of $\mathbf{T}$ are $D_{5/2}{}^+$, $D_{3/2}{}^+$, and $D_{1/2}{}^+$. Making use of the compatibility tables,[48] one finds that the $D_{5/2}{}^+$, $D_{3/2}{}^+$, and $D_{1/2}{}^+$ of the full rotation group decompose into $\Gamma_7+\Gamma_8$, Γ_8, and Γ_6, respectively, of $\bar{T}_d$. Thus, corresponding to a given p-like hydrogenic state there will be in general two fourfold Γ_8 states, one twofold Γ_6 state, and one twofold Γ_7 state. The results for 1s and np levels are summarized in Table I for both the $p_{1/2}$ and $p_{3/2}$ valence bands. This approach implicitly assumes that states associated with a given band are constructed exclusively from states of that band.

Schechter[46,47] has calculated the energies of the 1s level and the 2p levels associated with the $p_{3/2}$ valence band. These results will be discussed in Sec. IV and compared with the present experimental results.

B. Behavior of Acceptor States Under Uniaxial Stress

The top of the $p_{3/2}$ valence band, and many of the localized states associated with it are fourfold degenerate. For both, the set of four degenerate wave functions transform like a basis for a state of angular momentum $\mathbf{J}=\frac{3}{2}$. This fourfold degeneracy can be lifted partially by uniaxial stress on the crystal. The perturbing Hamiltonian describing the behavior of the $p_{3/2}$ valence band under small stress has been given by Kleiner and Roth[49] in terms of the angular-momentum

---

[43] R. J. Elliott, Phys. Rev. **96**, 266 (1954).

[44] C. Kittel and A. H. Mitchell, Phys. Rev. **96**, 1488 (1954).

[45] J. M. Luttinger and W. Kohn, Phys. Rev. **97**, 869 (1955).

[46] D. Schechter, Ph.D. thesis, Carnegie Institute of Technology, 1958 (unpublished).

[47] D. Schechter, J. Phys. Chem. Solids **23**, 237 (1962).

[48] G. F. Koster, J. O. Dimmock, R. G. Wheeler, and H. Statz, *Properties of the Thirty-Two Point Groups* (MIT Press, Cambridge, Massachusetts, 1965).

[49] (a) W. H. Kleiner and L. M. Roth, Phys. Rev. Letters **2**, 334 (1959). (b) G. L. Bir, E. I. Butikov, and G. E. Pikus, J. Phys. Chem. Solids. **24**, 1467 (1963).

operator **J** for $J=\frac{3}{2}$. This calculation predicts that under an applied force F the $m_j=\pm\frac{3}{2}$ states separate by Δ from the $m_j=\pm\frac{1}{2}$ states according to[49,50]

$$\delta E_{\pm 3/2}=\pm\tfrac{1}{2}\Delta=\pm\tfrac{2}{3}D_u(s_{11}-s_{12})T\,,$$
$$\delta E_{\pm 1/2}=\mp\tfrac{1}{2}\Delta=\mp\tfrac{2}{3}D_u(s_{11}-s_{12})T\,,\quad \text{for}\quad \mathbf{F}\|\langle 100\rangle\,,$$

and by Δ', according to (4)

$$\delta E_{\pm 3/2}=\pm\tfrac{1}{2}\Delta'=\pm\tfrac{2}{3}D_u'(\tfrac{1}{2}s_{44})T\,,$$
$$\delta E_{\pm 1/2}=\mp\tfrac{1}{2}\Delta'=\mp\tfrac{2}{3}D_u'(\tfrac{1}{2}s_{44})T\,,\quad \text{for}\quad \mathbf{F}\|\langle 111\rangle\,,$$

where the plus and minus signs refer to an increase and a decrease in electron energy, respectively; D_u and D_u' are the deformation potential constants of the valence band for uniaxial stress along the $\langle 100\rangle$ and $\langle 111\rangle$ directions, respectively; s_{11}, s_{12}, and s_{44} are the elastic compliance constants, and T, the resultant stress, is defined to be positive for tensile force. For $\mathbf{F}\|\langle 100\rangle$ and $\mathbf{F}\|\langle 111\rangle$, m_j remains a good quantum number, whereas for $\mathbf{F}\|\langle 110\rangle$, m_j is not a good quantum number in general[50] and the expression for the splitting involves both D_u and D_u'. Since the splittings given by Eq. (4) have been deduced from the symmetry of the valence band, similar relationships should hold for the splittings of the acceptor impurity states [see Ref. 49(b)]; of course, in principle, the values of D_u and D_u' will be different for each state.

It is possible to deduce the symmetries of the stress-induced sublevels on the basis of symmetry arguments. From these symmetry assignments, using standard group-theoretical techniques, it is then possible to deduce the selection rules for optical transitions between these sublevels. For a compressive force parallel to $\langle 100\rangle$, $\langle 111\rangle$, and $\langle 110\rangle$ the site symmetry is reduced to D_{2d}, C_{3v}, and C_{2v}, respectively. Compatibility relations between the irreducible representations of $\bar{T}_d$ and the irreducible representations of its subgroups then determine the behavior of the various states under uniaxial stress. This behavior is shown in Fig. 2 for $\mathbf{F}\|\langle 100\rangle$ and $\mathbf{F}\|\langle 111\rangle$. Also shown are the allowed electric dipole transitions for the electric vector **E**, either parallel or perpendicular to **F**. For $\mathbf{F}\|\langle 110\rangle$, Γ_6, Γ_7, and Γ_8 of $\bar{T}_d$ become Γ_5, Γ_5, and $2\Gamma_5$ of $\bar{C}_{2v}$, respectively. The selection rules, in this case, permit all transitions for both directions of polarization and all directions of **q**, the direction of light propagation, although for the orthorhombic point group a **q** dependence of the intensities for **E** perpendicular to **F** can be expected in general.

It is thus seen that states with Γ_8 symmetry split into two twofold degenerate states. The levels under stress retain the twofold spin degeneracy as is required by Kramers's theorem.[51] Thus the Γ_5 and Γ_6 of $\bar{C}_{3v}$ are degenerate and the twofold degeneracy of Γ_6 and Γ_7 of $\bar{T}_d$ is not lifted by uniaxial stress.

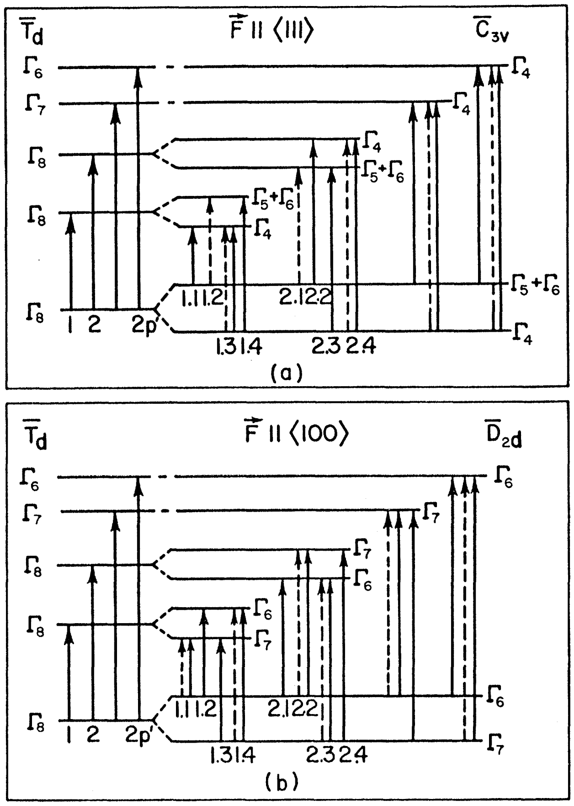

FIG. 2. The allowed transitions from a Γ_8 ground state to Γ_6, Γ_7, and Γ_8 excited states of the double group $\bar{T}_d$ with compressive force **F** along $\langle 111\rangle$ or $\langle 100\rangle$. The site symmetry is C_{3v} and D_{2d} for the $\langle 111\rangle$ and $\langle 100\rangle$ compressions, respectively; the designations next to the levels denote the irreducible representations of the appropriate double point group following the notation of Ref. 48. The dashed arrows are for the electric vector $\mathbf{E}\|\mathbf{F}$ while the full arrows are for $\mathbf{E}\perp\mathbf{F}$.

It is also possible to deduce relative intensities of the stress-induced components of a given transition from symmetry considerations. A procedure for carrying this out has been given by Kaplyanskii.[52] In this procedure, the symmetries of the initial and final states and that of the perturbing Hamiltonian are assumed to be known. The intensity of a given component of a stress induced multiplet is given by

$$I_\alpha\propto\sum_{k,l}\Big|\sum_{m,n}a_{km}{}^*b_{ln}\sum_{i=x,y,z}\alpha_i\langle\psi_m{}^*d_i\psi_n\rangle\Big|^2\,, \tag{5}$$

where the index α in I_α defines the direction of polarization of the light; d_i are the components of the dipole operator resolved along the crystal axes x, y, and z; α_i are the direction cosines of these components with respect to the directions defined by α. The coefficients a_{km} and b_{ln}, which have been tabulated by Kaplyanskii, determine the perturbed wave function in terms of the unperturbed wave functions ψ_m and ψ_n of the excited

---

[50] J. C. Hensel and G. Feher, Phys. Rev. **129**, 1041 (1963).

[51] V. Heine, *Group Theory in Quantum Mechanics*, (Pergamon Press, Inc., New York, 1960), p. 164.

[52] A. A. Kaplyanskii, Opt. i Spektroskopiya **16**, 1031 (1964) [English transl.: Opt. Spectry. **16**, 557 (1964)].

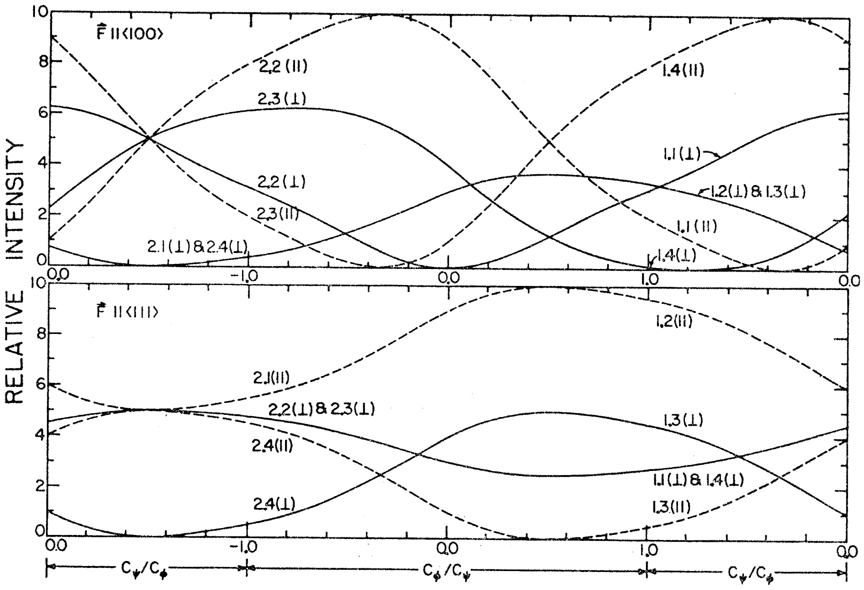

FIG. 3. Calculated relative intensities of the transitions between the stress induced sublevels of two Γ_8 states for uniaxial stress along either ⟨100⟩ or ⟨111⟩ as a function of the ratio of the undetermined parameters C_ϕ and C_ψ discussed in the text in Sec. IIIB. Note that the range $|C_\phi/C_\psi|>1$ has been plotted as C_ψ/C_ϕ.

and ground states, respectively; i.e.,

$$\psi_k=\sum_m a_{km}\psi_m,$$

and

$$\psi_l=\sum_n b_{ln}\psi_n. \tag{6}$$

The indices k and l denote the kth component of the final and the lth component of the initial states, respectively. The integrals $\langle\psi_m{}^*d_i\psi_n\rangle$ can be evaluated using the coupling coefficients conveniently tabulated by Koster *et al.*[48] A number of undetermined parameters enter in the evaluation of the matrix element of the dipole moment in this fashion. The number of such parameters is equal to the number of times the identity representation occurs in the product representation of the matrix element. (See Ref. 51, p. 103). In the case of the transition $\Gamma_8\rightarrow\Gamma_6$ (or Γ_7) one such parameter occurs, whereas for a $\Gamma_8\rightarrow\Gamma_8$ transition two parameters are needed.

Using Eq. (5), the relative intensities of the transitions shown in Fig. 2 have been calculated.[52] The components of the $\Gamma_8\rightarrow\Gamma_6$ transition have the relative intensities 3:1:4 for

$$(\Gamma_5+\Gamma_6\rightarrow\Gamma_4)_\perp:(\Gamma_4\rightarrow\Gamma_4)_\perp:(\Gamma_4\rightarrow\Gamma_4)_\parallel$$

in $\bar{C}_{3v}$, and

$$(\Gamma_6\rightarrow\Gamma_6)_\perp:(\Gamma_7\rightarrow\Gamma_6)_\perp:(\Gamma_7\rightarrow\Gamma_6)_\parallel$$

in $\bar{D}_{2d}$, respectively. Here the subscripts ⊥ and ∥ denote the direction of polarization. The intensity ratio of the components of $\Gamma_8\rightarrow\Gamma_7$ are the same as for the corresponding transitions for $\Gamma_8\rightarrow\Gamma_6$. The relative intensities for the $\Gamma_8\rightarrow\Gamma_8$ transitions for **F**∥⟨111⟩ and ⟨100⟩ are plotted in Fig. 3 as a function of the ratio of the undetermined parameters C_Ψ and C_ϕ which multiply the coupling coefficients corresponding to the two sets of

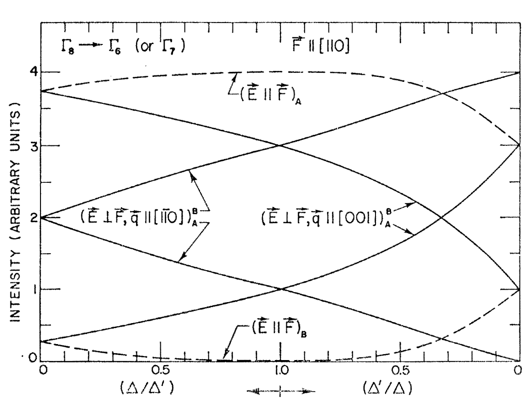

FIG. 4. Calculated relative intensities of the transitions between the stress induced sublevels of a Γ_8 state and a Γ_6 or Γ_7 state as a function of the ratio Δ'/Δ, where Δ' and Δ are the splittings of the Γ_8 state, given by Eq. (4). Note that the range $(\Delta'/\Delta)>1$ has been plotted as Δ/Δ'.

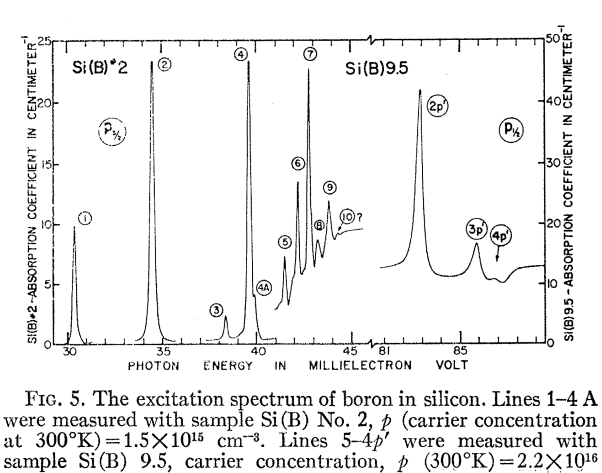

FIG. 5. The excitation spectrum of boron in silicon. Lines 1–4 A were measured with sample Si(B) No. 2, p (carrier concentration at 300°K) $=1.5\times10^{15}$ cm^{-3}. Lines 5–4p' were measured with sample Si(B) 9.5, carrier concentration, p (300°K) $=2.2\times10^{16}$ cm^{-3}. Liquid helium was used as coolant.

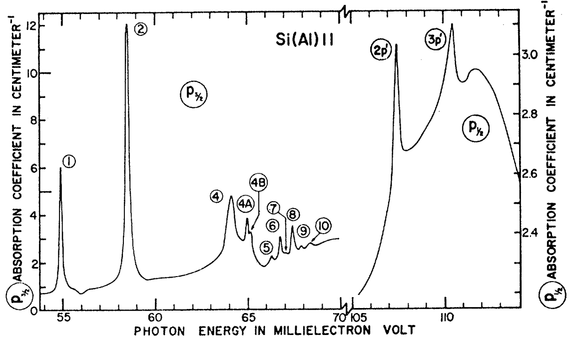

FIG. 6. The excitation spectrum of aluminum in silicon measured with liquid helium as coolant; $p(300°\mathrm{K})=2.7\times10^{15}$ cm^{-3}.

basis functions ψ and ϕ, respectively, used by Koster *et al.* (See Ref. 48, Table 83, p. 95.).

In the case of $\mathbf{F}\|\langle110\rangle$, the coefficients in Eq. (6) depend upon the ratio Δ'/Δ, where Δ' and Δ are defined in Eq. (4). Thus, as can be seen from Eq. (5), the intensities for this direction of compression will be a function of this ratio. Figure 4 shows the behavior of the intensity as a function of Δ'/Δ for the transition $\Gamma_8\rightarrow\Gamma_6$ (or Γ_7), where the components A and B denote the two possible transitions between the two sublevels of the Γ_8 state and the Γ_6 (or Γ_7) state which is not split by the stress. The relative intensities of the transitions between the sublevels of two Γ_8 states involve two splitting parameter (Δ'/Δ), one for each Γ_8 state, as well as the parameter C_ϕ/C_Ψ. In view of the uncertainties involved in such a calculation, a detailed comparison with experiment has not proved to be meaningful, and thus the detailed results of such an intensity calculation are not presented.

IV. EXPERIMENTAL RESULTS

A. Zero-Stress Spectra

The zero-stress spectra for boron, aluminum, gallium, and indium impurities in silicon are shown in Figs. 5–9. Both the $p_{3/2}$ and $p_{1/2}$ spectra are shown in each case.

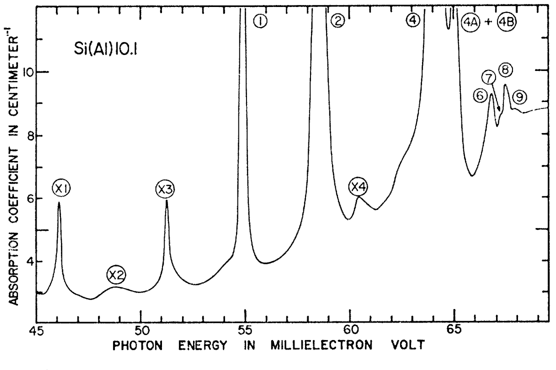

FIG. 7. The excitation spectrum of aluminum in crucible grown silicon showing the "extra lines" $X1$–$X4$; $p(300°\mathrm{K})=1.6\times10^{16}$ cm^{-3}. Liquid helium was used as coolant.

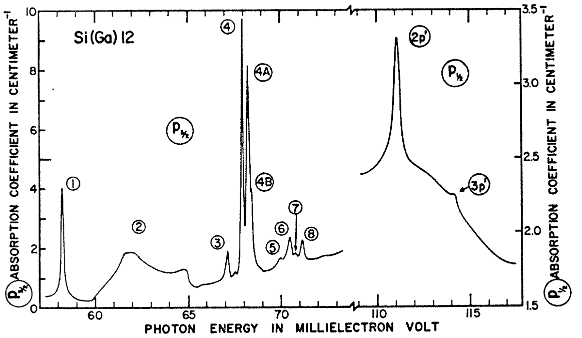

FIG. 8. The excitation spectrum of gallium in silicon measured with liquid helium as coolant; $p(300°\mathrm{K})=2.6\times10^{15}$ cm^{-3}.

The excitation lines observed have been labeled in the order of increasing energy; this notation has been employed by Colbow[11] for the case of boron. The lines of the $p_{1/2}$ spectrum have been designated by the notation of Zwerdling *et al.*[8]

1. Boron

The boron spectrum shown in Fig. 5 was obtained using samples of two different impurity concentrations. Both samples were floating-zone material. Lines 1–4A were obtained using the lower concentration sample and lines 5–10 and $2p'$–$4p'$ were measured with the sample of higher concentration. This spectrum has been studied previously by several investigators, the most recent of whom was Colbow.[11] The present results differ from those of Colbow in that many features are better resolved. For example, the high-energy shoulder on line 4 reported by Colbow has been clearly resolved and is labeled 4A in Fig. 5. The $p_{1/2}$ spectrum is essentially the same as that observed by Zwerdling *et al.*,[8] with some minor differences in the energies of the lines. The positions of all the observed lines are given in Table II.

2. Aluminum

The spectrum shown in Fig. 6 was obtained from floating-zone material. This spectrum is to be compared

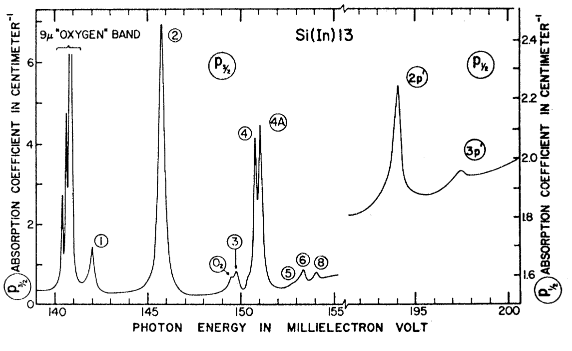

FIG. 9. The excitation spectrum of indium in crucible grown silicon measured with liquid helium as coolant; $p(300°\mathrm{K})=1.6\times10^{16}$ cm^{-3}.

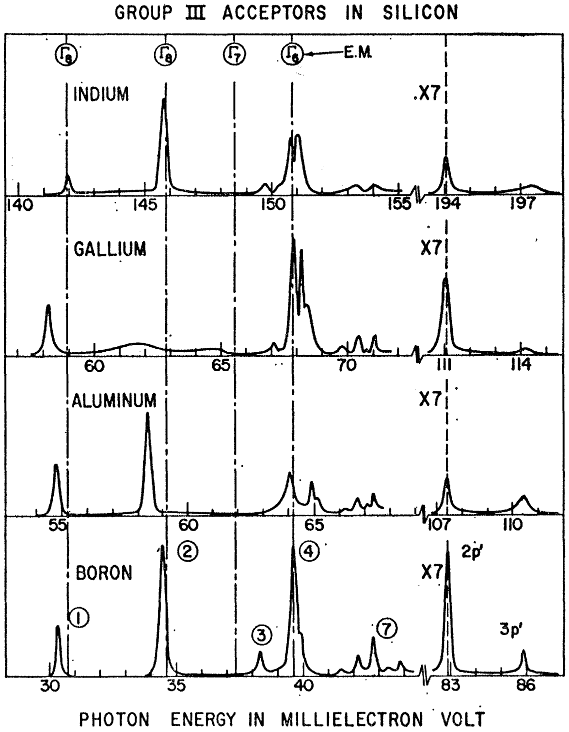

FIG. 10. Sketch of the group-III acceptor excitation spectra in silicon. The sketch shows the positions of the lines accurately. The relative intensities of the lines within a given spectrum are representative; note that the intensities of the $p_{1/2}$ lines compared to those of the $p_{3/2}$ lines have been scaled up by a factor of 7. The $2p'$ lines of the various spectra have been brought into coincidence, and the discontinuities in the horizontal scales have the same magnitude. The effective-mass excited states calculated by Schechter (see Ref. 47) for $B<0$ are also shown; the Γ_6 state has been aligned with line 4 of the boron spectrum.

with the previous measurements of Hrostowski and Kaiser,[7] and Zwerdling *et al.*[9] The line reported by these workers at ~65.0 meV has been, in the present measurements, resolved into two components labeled 4A and 4B in Fig. 6. The two lines $2p'$ and $3p'$ have been reported previously by Zwerdling *et al.*[8] In Fig. 6 these lines appear superimposed on a background of a lattice band. The energies of all the lines observed in the present measurements are listed in Table II. The weak lines 9 and 10 occur near strong water-vapor absorption bands, and thus their existence has not been established beyond doubt.

TABLE II. Experimental zero-stress positions of acceptor excitation lines in silicon.

Line No.	Boron[b]	Impurity line positions (meV)[a] Aluminum[b]	Gallium[b]	Indium[c]
1	30.38	54.88	58.23	141.99
2	34.53	58.49		145.79
3	38.35		67.12	149.74
4	39.64	64.08	67.95	150.80
4*A*	39.91	64.96	68.25	151.08
4*B*		65.16	68.43	
5	41.52	66.28	69.85	(152.8)
6	42.50	66.75	70.49	153.27
7	42.79	(67.1)	(70.8)	
8	43.27	67.39	71.11	153.97
9	43.86	(67.9)		
10	(44.32)	(68.4)		
$2p'$	82.90±0.03	107.48±0.03	111.11±0.03	194.07±0.06
$3p'$	85.89±0.03	110.46±0.05	114.20±0.05	197.41±0.15

[a] Energies in parentheses indicate weak or doubtful lines.
[b] Maximum error estimated to be ±0.02 meV.
[c] Maximum error estimated to be ±0.03 meV.

The $p_{3/2}$ spectrum obtained from a crucible grown aluminum doped sample is shown in Fig. 7. The impurity concentration is about 10 times that of the sample from which the results of Fig. 6 were obtained. In addition to the lines 1–10 seen in Fig. 6, this spectrum exhibits the lines X1–X4 at the energies ~46.12, 48.8, 51.26, and 60.5 meV, respectively. These lines have not been observed in floating-zone material. These additional lines are not seen at liquid-nitrogen and room temperatures.

3. *Gallium*

The spectrum of gallium in floating-zone silicon is shown in Fig. 8. The increased resolution of the present measurements has revealed much more detail for the line at 68.26 meV reported by Hrostowski and Kaiser,[7] viz., the single line previously reported has been clearly resolved into two sharp lines and a well-defined shoulder. The $p_{1/2}$ spectrum of gallium in silicon has not been reported previously. It appears on the same lattice band as does the $p_{1/2}$ spectrum of aluminum. The positions of the lines are given in Table II.

4. *Indium*

The $p_{3/2}$ and $p_{1/2}$ excitation spectra of indium impurity in silicon are presented in Fig. 9. The $p_{1/2}$ spectrum has not been reported previously. In the present measurements, the $3p'$ line is very weak, and thus several measurements were made to determine its position. As has been found for the other three impurities, line 4 again shows more detail than previously reported. In this case, the line reported at 150.88 meV by Hrostowski and Kaiser[7] has been resolved into two sharp lines designated in Fig. 9 by 4 and 4A. The material used in this measurement was crucible-grown silicon, as is evident from the presence of the 9μ "oxygen band" and the weak line at 149.48 meV to the low-energy side of line 3.[53] The positions of the lines are given in Table II.

5. *Discussion of Experimental Results for Zero Stress*

A comparison of the excitation spectra of the four impurities studied is given schematically in Fig. 10.

---

[53] It is well known that the 9-μ band exhibits strong temperature effects [H. J. Hrostowski and R. H. Kaiser, Phys. Rev. **107**, 966 (1957)]. A detailed investigation of the temperature dependence of the 9-μ band has been made by R. L. Aggarwal, B. T. Ahlburn, and A. K. Ramdas (private communication). This study shows that in the range 10–25°K, there is rapid growth of a component at 139.87 meV; the strength of this line has been used to gauge the temperature. This line is missing in Fig. 9, hence it is concluded that the temperature for that measurement is less than 10°K.

In this figure, the $2p'$ lines of the different impurities have been brought into coincidence. The energy scales of the spectra are the same and the discontinuity between each $p_{3/2}$ and $p_{1/2}$ spectrum is also the same. Included in the sketch are the energy spacings calculated by Schechter.[46,47] The correlation between theory and experiment has been made by assuming that the final state of line 4 coincides with the Γ_6 state calculated by Schechter, with the effective-mass parameter $B<0$.[50] As remarked above, the experimentally observed $2p'$ line has been used as a reference in Fig. 10. It is found that when the $2p'$ lines of the various spectra are brought into coincidence, an optimum correspondence between the features of the various spectra is achieved. Indeed, the $2p'$ line also seems a reasonable choice as a reference line for acceptors in silicon since the chemical species dependence of its binding energy is small (see Table III). However, it should be noted that, on the basis of the calculated positions of the $p_{1/2}$ valence band edge in Table III, the gallium and indium spectra of Fig. 10 would be moved somewhat to lower energies if the $p_{1/2}$ valence band were used as a reference.

The general similarity among the spectra is evident in that lines or complexes of lines are observed in corresponding positions. However, there are noticeable species-dependent features. The most striking of these is the variation in structure of the line 4 complex. Also, the line 1 to line 2 spacings, although close to the effective-mass value, do show species-dependent variations. Another remarkable feature is the absorption consisting of two broad peaks in the gallium spectrum in the region where line 2 is expected (see also Fig. 8). Also, line 3 is missing in the spectrum of aluminum impurity. It should be noted that both these lines are expected to occur at about 63 meV, an energy which is close to that of the optical phonons of silicon.[54] This suggests that the anomalous features of the gallium and aluminum spectra may be due to interaction with optical phonons. This is an alternative explanation to that suggested by Hrostowski and Kaiser,[7] who have proposed that "The broadening of the 498.6-cm^{-1} gallium frequency apparently results from an interaction of the silicon-oxygen bending mode with the electronic transition of a bound hole from the ground state to the second excited state of gallium." This will be discussed in more detail elsewhere.

The occurrence of the spectra of the different group-III acceptors in different spectral regions is a well-known feature for acceptors and donors in silicon and germanium; it is due to the chemical shift of the ground state. However, what is surprising is the chemical species dependence of the $p_{3/2}$ lines, as discussed above. Such an effect has not been observed either for acceptors in germanium,[55–59] or for donors in silicon[18,20,60] and germanium.[61] It should also be noted that the effective-mass calculation predicts a line in the region between lines 2 and 3 (see Fig. 10); this is not observed in any of the spectra except possibly for gallium. It will be shown in Sec. IV B that the final state of line 3 has Γ_8 symmetry, hence this line is not due to the predicted Γ_7 state.

TABLE III. Ionization limit[a] of the $p_{1/2}$ series and binding energy of the $2p'$ line. Units are meV.

	Impurity			
	B	Al	Ga	In
ϵ_I^*	88.35±0.18	112.93±0.18	116.74±0.21	200.16±0.40
ϵ_I^*-2p'	5.45±0.15	5.45±0.15	5.63±0.18	6.09±0.34

[a] Energy necessary to ionize a hole from the ground state associated with the $p_{3/2}$ valence band to the $p_{1/2}$ valence band. The uncorrected Rydberg series given by Zwerdling *et al.* (Ref. 8) has been used to estimate ϵ_I^*.

The ionization energy of an acceptor relative to the $p_{3/2}$ valence band can be calculated by adding the effective-mass binding energy[47] of a state to the observed energy of excitation to that state. For example, if the final state of line 4 of boron is assumed to include the Γ_6 effective-mass excited state, then the transition from the $p_{3/2}$ ground state to the $p_{3/2}$ valence band edge would occur at 44.04±0.12 meV. This energy lies between the energies of lines 9 and 10 of Fig. 5, indicating that the $p_{3/2}$ ionization energy probably occurs at a somewhat higher value. Thus the effective-mass binding energy of the Γ_6 excited state appears to be somewhat small.

In Table III, the energy difference between the $p_{3/2}$ ground state and the $p_{1/2}$ valence band edge for different impurities are given. These energies have been estimated assuming the Rydberg formula for the $p_{1/2}$ series used by Zwerdling *et al.*[8] These authors have also calculated the spin-orbit splitting of the valence band in silicon. This has been obtained on the basis of their estimate of 88.2±0.1 meV for the position of the $p_{1/2}$ valence band with respect to the $p_{3/2}$ ground state of boron, and a "series-limit" of 44.1±0.3 meV for the $p_{3/2}$ spectrum deduced from the data of Hrostowski and Kaiser.[7] From the present data, these values are estimated to be 88.35±0.18 and ≥ 44.32 meV, respectively; here the $p_{3/2}$ ionization energy is assumed to be at an energy greater or equal to that of line 10. From the present data, the spin-orbit splitting is estimated to be $\leq 44.0 \pm 0.2$ meV. This is to be compared with 44.1±0.4 meV deduced by Zwerdling *et al.*[8] Clearly, better calculations of the energies of the localized states are necessary before

---

[54] B. N. Brockhouse, Phys. Rev. Letters **2**, 256 (1959); F. A. Johnson, in *Progress in Semiconductors*, edited by A. F. Gibson and R. Burgess (Temple Press Books Limited, London, 1965), Vol. 9, p. 179.

[55] R. L. Jones and P. Fisher, J. Phys. Chem. Solids **26**, 1125 (1965).

[56] W. J. Moore and R. Kaplan, Bull. Am. Phys. Soc. **11**, 206 (1966).

[57] P. Fisher and H. Y. Fan, Phys. Rev. Letters **5**, 195 (1960).

[58] W. J. Moore, Solid State Commun. 3, 385 (1965).

[59] R. A. Chapman and W. G. Hutchinson, Solid State Commun. 3, 293 (1965).

[60] R. L. Aggarwal, Ph.D. thesis, Purdue University, 1965 (unpublished).

[61] J. H. Reuszer and P. Fisher, Phys. Rev. **135**, A1125 (1964).

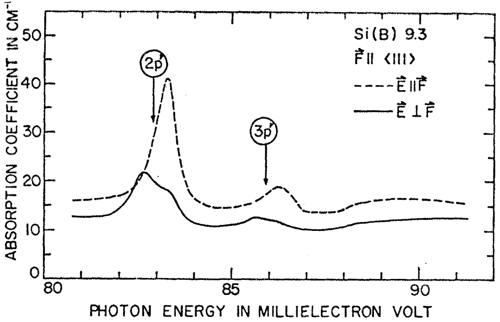

FIG. 11. The effect of a ⟨111⟩ compression on the $p_{1/2}$ spectrum of boron in silicon. Liquid helium was used as coolant; $p(300°K) = 2.2\times10^{16}$ cm^{-3}. The encircled numbers together with the vertical arrows designate the zero stress positions of the lines.

an accurate determination of the spin-orbit splitting of the valence band can be made from such measurements.

B. Effect of Uniaxial Stress

In this section the behavior of the excitation spectra of group-III acceptors under uniaxial compression is presented. Observations have been made with **F** along ⟨100⟩, ⟨111⟩, or ⟨110⟩, and the electric vector **E** of the polarized radiation either parallel or perpendicular to **F**. In the case of **F**∥[110], the measurements have been made with the direction of propagation of the light **q** along either [1$\bar{1}$0] or [001].

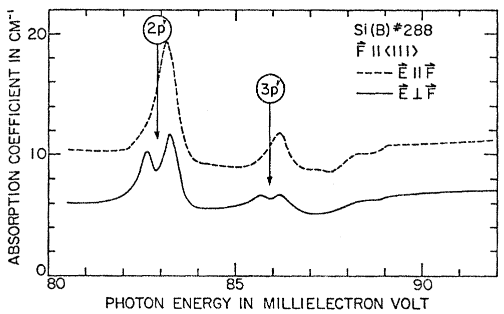

FIG. 12. The effect of a ⟨111⟩ compression on the $p_{1/2}$ spectrum of boron in silicon. Liquid helium was used as coolant; $p(300°K) = 1.1\times10^{16}$ cm^{-3}.

1. *Boron*

The effect of a ⟨111⟩ compression on the $p_{1/2}$ spectrum of boron in silicon is presented in Figs. 11, 12, and 13. As can be seen in Fig. 12, both the $2p'$ and $3p'$ lines split into two components. The high-energy components are observed for both directions of polarization, while the low-energy components are seen only for **E**⊥**F**. For this direction of compression, the effects of a smaller and a larger stress are shown in Figs. 11 and 13, respectively; the relative magnitudes of the stresses are inferred from the experimental conditions. Since the temperature for the measurements is estimated to be the same, the decrease in intensity of the low-energy perpendicular components of both the $2p'$ and $3p'$ lines with respect to the corresponding high-energy perpendicular components indicates that the splitting of the spectral lines is due to a splitting of the ground state. Thus it is assumed that the ground state splits into two levels, the upper being depopulated with increasing stress. It may also be noted that there is a distinct difference in the background absorption for the two directions of polarization. The existence of this feature has been established from many measurements. The origin of this effect has not been investigated.

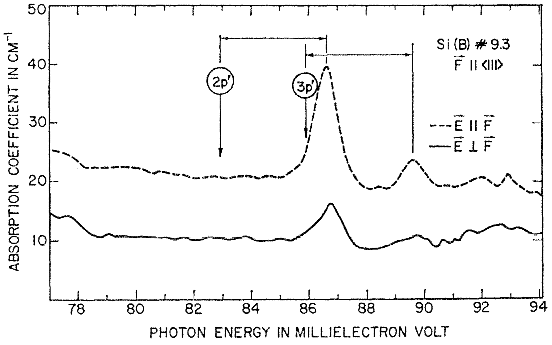

FIG. 13. The effect of a large ⟨111⟩ compression on the $p_{1/2}$ spectrum of boron in silicon. Liquid helium was used as coolant; $p(300°K) = 2.2\times10^{16}$ cm^{-3}.

The behavior of the $p_{1/2}$ spectrum under compression along ⟨100⟩ is shown in Fig. 14, while Figs. 15 and 16 present similar results for **F**∥[110] for **q**∥[1$\bar{1}$0] and **q**∥[001], respectively. The number of components and their polarization characteristics are identical to those for **F**∥⟨111⟩. Depopulation effects of the same type as for **F**∥⟨111⟩ have also been observed.

The ground state of the $p_{1/2}$ series has been shown by Zwerdling *et al.*[8] to be the ground state associated with the $p_{3/2}$ valence band. According to Schechter,[46,47] this is a fourfold degenerate state of Γ_8 symmetry. Thus, under uniaxial stress the ground state is expected to split into two sublevels. The appearance of the two stress-induced components of the $p_{1/2}$ lines, together with the depopulation effects, is consistent with transitions from a Γ_8 ground state to Γ_6 or Γ_7 excited states (see Sec.

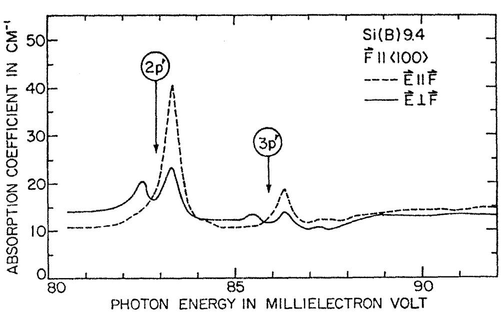

FIG. 14. The effect of a ⟨100⟩ compression on the $p_{1/2}$ spectrum of boron in silicon. Liquid helium was used as coolant; $p(300°K) = 2.2\times10^{16}$ cm^{-3}.

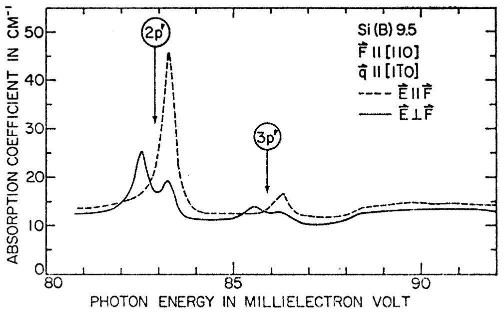

FIG. 15. The effect of a [110] compression on the $p_{1/2}$ spectrum of boron in silicon for the direction of light propagation $\mathbf{q}\|[1\bar{1}0]$. Liquid helium was used as coolant; $p(300°\text{K})=2.2\times10^{16}$ cm^{-3}.

IIIB). However, as is shown in Table I, the theory predicts only Γ_6 excited states to be associated with the $p_{1/2}$ valence band. Thus it is assumed that the excited states of the $2p'$ and $3p'$ lines are Γ_6 states.

In Fig. 17 is shown the effect of compression along $\langle111\rangle$ for lines 1–4 of the $p_{3/2}$ spectrum and the $2p'$ line of the $p_{1/2}$ spectrum. The insets show the behavior of lines 1 and $2p'$ under a stress larger than that of the main figure. It is found that the spacings 1.1–1.3, 1.2–1.4, 2.1–2.3, and 2.2–2.4 are the same and equal to the splitting of the $2p'$ line. Thus it is concluded that this common spacing represents the splitting of the common ground state. In addition, the low-energy components 1.1 and 1.2 show, qualitatively, the same depopulation effects as does the low-energy $2p'$ component. Similar behavior is observed for components 2.1 and 2.2. The decrease in intensity of these components is accompanied by corresponding increases in intensity of the high-energy components. A study of the weaker lines 3 and 5–9 is presented in Fig. 18 for $\mathbf{F}\|\langle111\rangle$; these results have been obtained with a sample of higher boron concentration than that of Fig. 17. It can be seen from both Figs. 17 and 18 that line 3 generates four components with a polarization pattern identical to that of line 1. Also, line 5 behaves in a fashion similar to lines 1 and 3. Lines 6 and 7 appear to give two and three components, respectively. Little can be said regarding the behavior of lines 8 and 9. The striking results observed for lines 4 and 4A will be discussed later in this section.

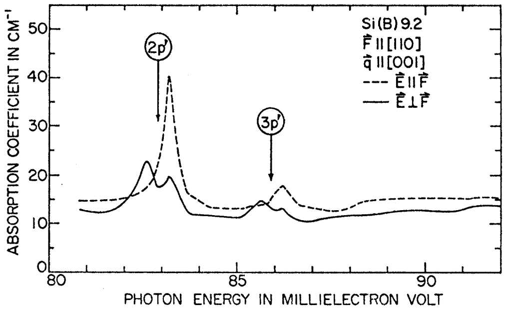

FIG. 16. The effect of a [110] compression on the $p_{1/2}$ spectrum of boron in silicon for $\mathbf{q}\|[001]$. Liquid helium was used as coolant; $p(300°\text{K})=2.2\times10^{16}$ cm^{-3}.

The above experimental results can be interpreted in terms of the selection rules given in Fig. 2. Independent of whether the final state of the $2p'$ line is of Γ_6 or Γ_7 symmetry, the polarization features of this line for $\mathbf{F}\|\langle111\rangle$ unambiguously order the sublevels of the split Γ_8 ground state. The ordering so deduced is that given in Fig. 2(a). A comparison of the experimental results for line 1 with the selection rules determines the symmetries and the ordering of the sublevels of the excited state of this line. These are also shown in Fig. 2 (a). The only discrepancy between the allowed and observed transitions is the occurrence of the component 1.4 in the parallel polarization. However, the existence of this

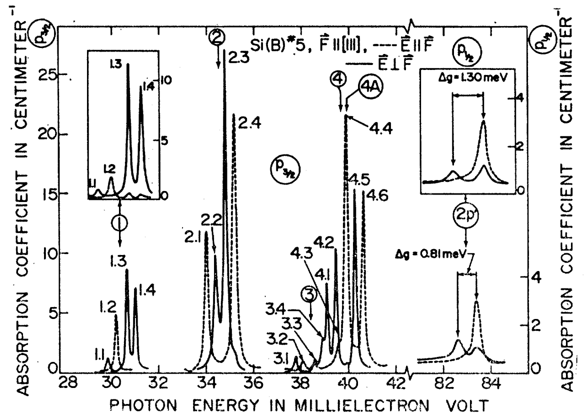

FIG. 17. The excitation lines 1–4A and $2p'$ of boron in silicon under a $\langle111\rangle$ compression. The two insets show the effect of a larger stress on the lines 1 and $2p'$. Liquid helium was used as coolant; $p(300°\text{K})=1.5\times10^{15}$ cm^{-3}.

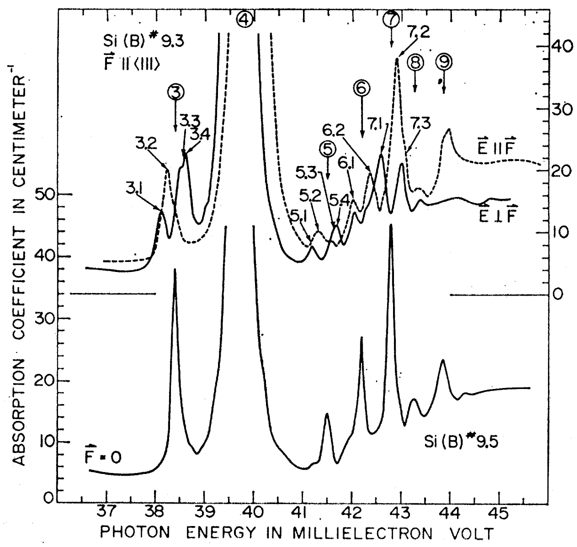

FIG. 18. The effect of a $\langle111\rangle$ compressive force on the lines 3, and 5–9 of the excitation spectrum of boron in silicon. The curve in the lower half of the figure is the zero-stress spectrum. Liquid helium was used as coolant; $p(300°\text{K})=2.2\times10^{16}$ cm^{-3}.

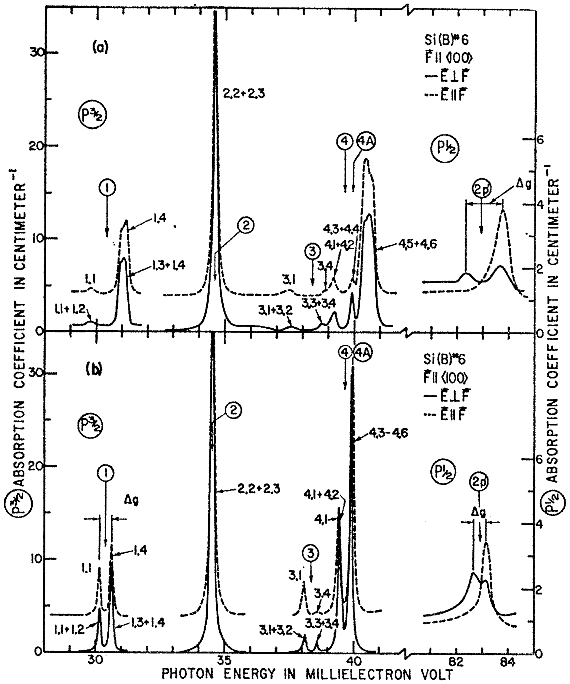

FIG. 19. The effect of a ⟨100⟩ compression on the excitation spectrum of boron in silicon for two magnitudes of compressive force. The stress in (a) is somewhat inhomogeneous. Liquid helium was used as coolant; $p(300°\mathrm{K})=1.5\times10^{15}$ cm^{-3}.

very weak component, as well as that of 1.3 in the parallel polarization, is in doubt since other measurements with samples of higher boron concentration fail to show either.

The polarization features observed for line 2 in Fig. 17 are clearly those for the Γ_8 to Γ_8 transitions 2.1–2.4 depicted in Fig. 2(a). It is interesting to note that the sublevels of the excited states of lines 1 and 2 are inverted with respect to each other. It should also be noted that, unlike line 1, the polarization pattern of line 2 gives a unique ordering of the sublevels of both the excited and ground states. However, this depends upon establishing, beyond doubt, the existence of the weak component 2.4 observed in the perpendicular polarization; measurements with a sample of higher boron concentration appear to confirm the existence of this component. The ordering thus obtained is the same as that deduced from the $2p'$ line.

The effect of compression along ⟨100⟩ is shown in Fig. 19. If the symmetry of the excited state of the $2p'$ line is chosen to be Γ_6, in agreement with the results given in Table I, then the experimental results order the sublevels of the ground state as shown in Fig. 2 (b). As can be seen from the figure, only two transitions are allowed in the parallel polarization for a Γ_8 to Γ_8 transition. These must be either extreme or intermediate components. The spacing of the parallel components 1.1 and 1.4 is the same, within experimental error, as the splitting of the $2p'$ line, i.e., the ground-state splitting. It is therefore deduced that the excited-state splitting is very small. In this case, either of the Γ_8 to Γ_8 transitions shown in Fig. 2 (b) is applicable to line 1. The two components of line 1 observed for $\mathbf{E}\perp\mathbf{F}$ are almost coincident with the two parallel components. The slightly smaller spacing of the perpendicular components compared to that of the parallel components indicates that the excited state of line 1 splits by a very small but finite amount. The Γ_8 to Γ_8 transition labeled as line 1 in Fig. 2 (b) has been selected on this basis.

The behavior of line 2 is remarkable in that only a component at the zero-stress position is observed for both directions of polarization. This is found to be the case for ⟨100⟩ compressions of various magnitudes. This behavior can be understood only if both the ground state and the excited state split by the same amount. That the ground state splits is clear from the behavior of lines 1 and $2p'$. Thus the observed transitions are a superposition of the intermediate components labeled 2.2 and 2.3 in Fig. 2(b). This interpretation is supported by the sharpness of line 2 in Fig. 19(a), where the broadness of the other lines indicates some inhomogeneity in the stress. The intermediate components 2.2 and 2.3, when the ground- and the excited-state splittings are the same, will be insensitive to inhomogeneity in the stress. The extreme components 2.1 and 2.4 are evidently very weak; however, with a sample of higher boron concentration, a very weak line has been observed at the position expected for the component 2.4.

The polarization pattern of line 3 is again similar to that of line 1, as was found to be the case for $\mathbf{F}\|\langle111\rangle$.

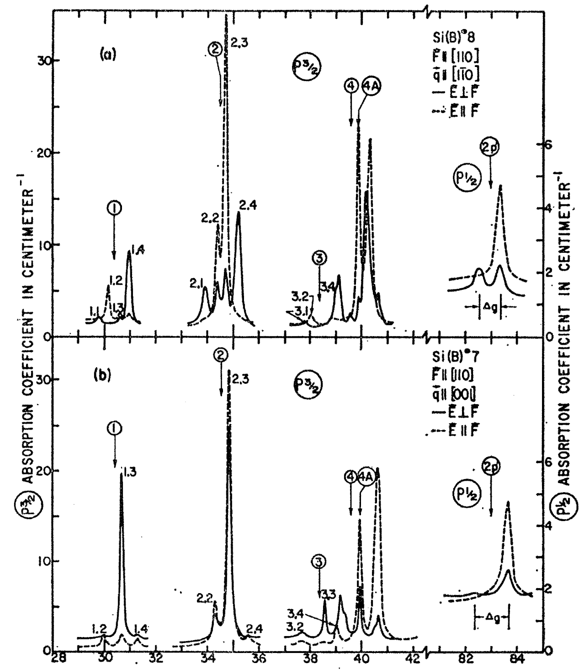

FIG. 20. The effect of a [110] compression on the excitation spectrum of boron in silicon for $\mathbf{q}\|[1\bar{1}0]$ and $\mathbf{q}\|[001]$. Liquid helium was used as coolant; $p(300°\mathrm{K})=1.5\times10^{15}$ cm^{-3}.

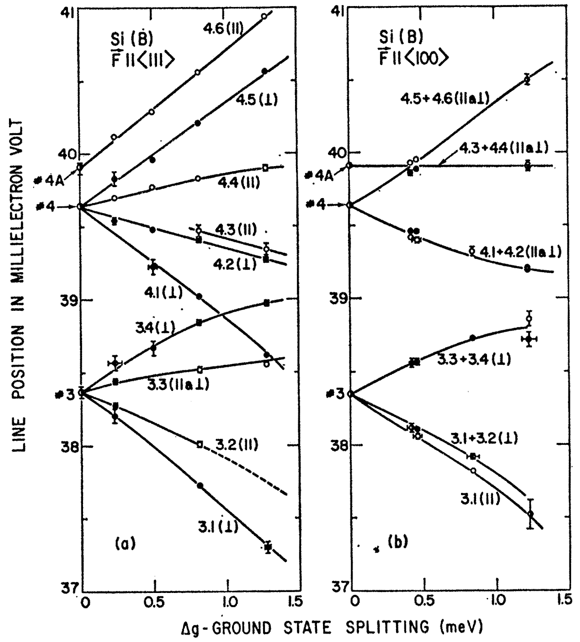

FIG. 21. Positions of the stress-induced components of lines 3, 4, and 4A of boron impurity in silicon as a function of ground-state splitting for a compressive force along either ⟨111⟩ or ⟨100⟩. The open circles designate lines observed for **E**||**F** and the full circles lines observed for **E**⊥**F**. For **F**||⟨100⟩, with $\Delta g=0.84$ meV, it was not possible to identify most of the components of lines 4 and 4A because of the large absorption of this line due to the high-impurity concentration.

However, the experimental results indicate that the excited state of line 3 splits somewhat more than that of line 1. The detailed discussion of lines 4 and 4A is given later in this section. It should be pointed out that in Fig. 19(a) the sharp component labeled 4.3+4.4 occurs at the zero-stress position of 4A and is unaffected by the inhomogeneous stress. This suggests that the excited state of 4A behaves in the same way as the excited state of line 2.

The behavior of the excitation spectrum of boron for compression along [110], **q**||[1$\bar{1}$0] and **q**||[001], is shown in Figs. 20(a) and 20(b), respectively. The following features can be noted. The spectra for **E**||**F** for both directions of **q** are the same, as expected. The spectra do, however, show a strong **q** dependence for **E**⊥**F**. For example, the components 1.3, 2.3, and 3.3, which are intense for **q**||[001], are weak for **q**||[1$\bar{1}$0]. On the other hand, the components 1.4, 2.4, and 3.4 are weak for **q**||[001] and strong for **q**||[1$\bar{1}$0]. Similar **q**-dependent features are observed for line 4. Again, lines 1 and 3 exhibit the same polarization pattern, but different from line 2. The number of components observed for these three lines is consistent with each being a $\Gamma_8 \to \Gamma_8$ transition, the final states of lines 1 and 2 behaving differently, however, under stress. In Figs. 20(a) and 20(b), the components of lines 4 and 4A have not been labeled in view of the complex behavior of these under a ⟨110⟩ compression.

The behavior of lines 3, 4, and 4A as a function of ground-state splitting for **F**||⟨111⟩ and **F**||⟨100⟩ is shown in Fig. 21. This diagram permits the components of lines 3 and 4 to be distinguished. The ground-state splitting, which has been obtained from line 1, line 2, or the $2p'$ line, depending on which gave the most precise determination, has been used as a gauge of the strain produced in the crystal by the compressive force. It is seen that for **F**||⟨111⟩ lines 4 and 4A produce six stress-induced components. For **F**||⟨100⟩, two components are seen for the smaller stress, and three for the larger stress.

In Fig. 21(a) the strong components 4.1, 4.2, 4.4, and 4.5 clearly extrapolate to the zero-stress position of line 4, while the component 4.6 extrapolates to that of line 4A. This appears to confirm that 4A is due boron impurity rather than incomplete cancellation of atmospheric water vapor absorption as speculated by Colbow.[11] It is found that the components 4.1 and 4.4 as well as the components 4.2 and 4.5 are separated by the ground-state splitting. Using depopulation effects as a further criterion, it is concluded that components 4.1 and 4.4 have the same final state; similarly components 4.2 and 4.5 have the same final state. The data for the weak component 4.3 are insufficient to determine whether it originates from 4 or 4A. However, its polarization is consistent with its final state being of Γ_8 symmetry. From the fact that line 4 exhibits four stress-induced components, neglecting 4.3, it might appear that line 4 results from a Γ_8 to Γ_8 transition. However, it can be shown that the polarization features of the components of line 4 can not be reconciled with either of the Γ_8 to Γ_8 transitions shown in Fig. 2(a). The simplest combination of excited states of line 4 that can be chosen, consistent with the observed polarization features, is $2\Gamma_6$, $\Gamma_6+\Gamma_7$, or $2\Gamma_7$, which separate with stress. Since only one component is seen for line 4A, it is not possible to identify the final state of this transition on the basis of its behavior under a ⟨111⟩ compression alone.

The behavior of lines 4 and 4A as a function of ground-state splitting for **F**||⟨100⟩ is shown in Fig. 21(b). The presence of the sharp component 4.3+4.4 in the spectrum of Fig. 19(a) under an inhomogeneous stress implies that, like 2.2+2.3, these are transitions to a Γ_8 state which splits by the same amount as the ground state. Since this line also occurs at the zero-stress position of 4A, it is concluded that it arises from 4A. Hence the final state of line 4A appears to be a Γ_8 state. The components 4.1+4.2 and 4.5+4.6 are separated by the ground-state splitting, and appear to be the only components arising from line 4. It is thus concluded that the accidental degeneracy of the two states which comprise the excited state of line 4 remains for **F**||⟨100⟩. Moreover, since both components 4.1+4.2 and 4.5+4.6 are observed in the parallel polarization, the selection rules of Fig. 2(b) demand that this state be $\Gamma_6+\Gamma_7$, rather than $2\Gamma_6$ or $2\Gamma_7$.

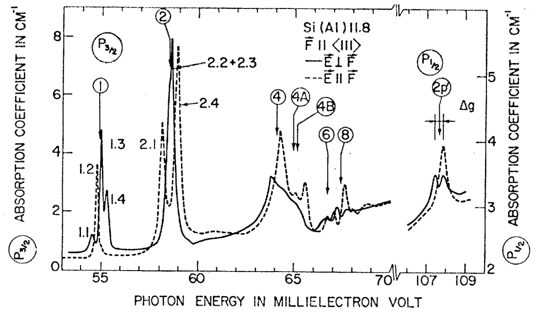

FIG. 22. The effect of a ⟨111⟩ compression on the excitation spectrum of aluminum in silicon. Liquid helium was used as coolant; $p(300°\mathrm{K})=2.7\times10^{15}$ cm^{-3}.

A comparison will now be made between the experimentally observed intensities of the stress-induced components and those given in Sec. III B. Experimentally it is observed that for $\mathbf{F}\|\langle111\rangle$ and ⟨100⟩, the high-energy component of the $2p'$ line, which is a $\Gamma_8\rightarrow\Gamma_6$ transition, has a larger intensity for the parallel polarization than for the perpendicular. Theoretically, this ratio is expected to be 4 to 1. The experimental observations are qualitatively in good agreement with this prediction, as can be seen in Figs. 11–14, 17, and 18. Similarly, theory predicts that the low-energy perpendicular component should be three times as intense as the high-energy perpendicular component. However, in order to make this comparison, the depopulation effects must be taken into account. Since the actual temperature is not well known, a quantitative comparison is not practical. However, with reasonable temperature estimates qualitative agreement with theory is obtained. For $\mathbf{F}\|\langle110\rangle$, the ratios of intensities are not unique, but vary as a function of Δ'/Δ for the ground state, as shown in Fig. 4. The splittings Δ' and Δ are defined in Eq. (4). As can be seen in Fig. 4, the component $(\mathbf{E}\|\mathbf{F})_B$ is expected to be very weak compared to $(\mathbf{E}\|\mathbf{F})_A$ over a wide range of values of Δ'/Δ. Thus, from the experimental results of Figs. 15 and 16, the component $(\mathbf{E}\|\mathbf{F})_A$ of Fig. 4 is identified as the high-energy component for lines $2p'$ and $3p'$. However, the fact that component B is not observed experimentally in the parallel polarization cannot be used to deduce a value for Δ'/Δ because a low intensity is predicted for this component over a large range of values for this ratio. The relative intensities of the perpendicular components or of the high-energy parallel and perpendicular components are more restrictive in the range of possible values of Δ'/Δ. For example, the present experimental results indicate that Δ'/Δ is probably within the range 0.75–1.33. Note that if $\Delta'/\Delta=1$, then the intensity ratios would be indistinguishable from those predicted for $\mathbf{F}\|\langle100\rangle$ and $\mathbf{F}\|\langle111\rangle$. For this case, with a given magnitude of applied force, the following relationship holds between deformation potential and elastic compliance constants:

$$D_u(s_{11}-s_{12})=D_u'(s_{44}/2)\,. \qquad (7)$$

Such a relationship between deformation-potential constants has been noticed by Hensel and Feher[50] in their studies of the effect of uniaxial stress on the cyclotron resonance of holes in silicon, and by Thomas[62] for the valence band of CdTe, in his investigation of the effect of uniaxial stress on the direct exciton. As pointed out above, a significant deviation from $\Delta'/\Delta=1$ can occur before it is reflected in the observed relative intensities of the stress-induced components of the $2p'$ line.

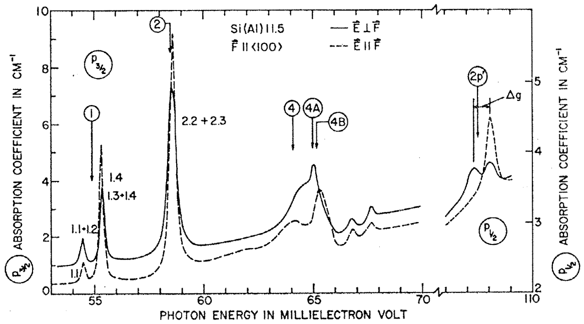

FIG. 23. The effect of a ⟨100⟩ compression on the excitation spectrum of aluminum in silicon. Liquid helium was used as coolant; $p(300°\mathrm{K})=2.7\times10^{15}$ cm^{-3}.

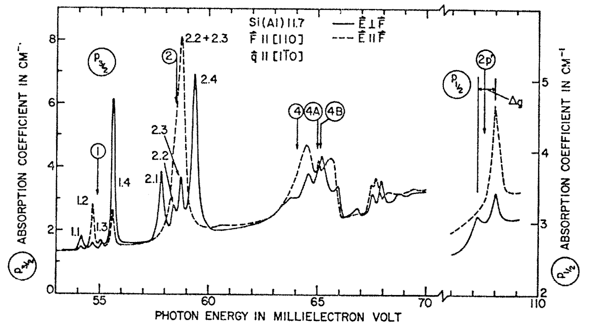

FIG. 24. The effect of a [110] compression on the excitation spectrum of aluminum in silicon for $\mathbf{q}\|[1\bar{1}0]$. Liquid helium was used as coolant; $p(300°\mathrm{K})=2.7\times10^{15}$ cm^{-3}.

The relative intensities of the stress-induced components of a Γ_8 to Γ_8 transition expected on the basis of symmetry have been given in Fig. 3 for $\mathbf{F}\|\langle100\rangle$ and $\mathbf{F}\|\langle111\rangle$. As pointed out earlier, if the wave functions of the levels participating in the transition are not known, the calculated relative intensities can be expressed only to within an arbitrary parameter C_ϕ/C_ψ. The calculations show that for $\mathbf{F}\|\langle111\rangle$, only one strong component is expected in the parallel polarization for a wide range of values of C_ϕ/C_ψ, i.e., between ~0 to ~1.3. This feature is in agreement with the behavior of line 1, which exhibits only one prominent component in the parallel polarization, viz., 1.2. The calculations also predict three components of comparable magnitude

---

[62] D. G. Thomas, J. Appl. Phys. 32, 2298 (1961).

in the perpendicular polarization, in agreement with experiment. In the case of line 2, the low intensity of component 2.4 in the perpendicular polarization can be accounted for if C_ϕ/C_ψ is chosen in the vicinity of -2. In the same range of C_ϕ/C_ψ, the presence of prominent parallel or perpendicular components of nearly equal intensity can be accounted for by the calculations. The above identification of the various branches with the observed components of line 2 is also consistent with the reversal of the ordering of the stress-induced sublevels of the excited states associated with lines 1 and 2. For $\mathbf{F}\|\langle 100\rangle$, the predicted intensities for line 1 in the range of values of C_ϕ/C_ψ consistent with the $\langle 111\rangle$ results do not contradict the experimental observations. For line 2, the calculations predict that, for the range of values of C_ϕ/C_ψ obtained from the $\langle 111\rangle$ data, the components 2.1 and 2.4 for $\mathbf{E}\perp\mathbf{F}$ should be nearly absent; this is consistent with the experimental results. In addition, 2.2+2.3 for both directions of polarization are predicted to be of comparable intensity, also in good agreement with the observations.

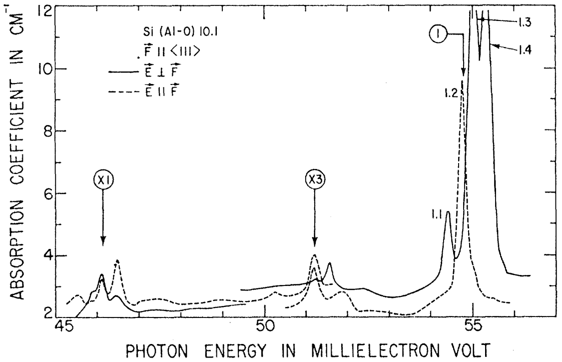

FIG. 25. The effect of a $\langle 111\rangle$ compression on the "extra lines" X1 and X3 and line 1 of aluminum in crucible grown silicon. Liquid helium was used as coolant; $p(300°\mathrm{K})=1.6\times10^{16}$ cm^{-3}.

A comparison of the observed intensities with those calculated has not been attempted in a detailed way for any of the remaining lines. However, an interesting feature regarding line 3 may be mentioned. Even though the stress behavior of this line, as far as selection rules go, is the same as that of line 1, the relative intensities of their components are different. This presumably can be attributed to a different value for the ratio C_ϕ/C_ψ for the two cases. Another interesting feature is the intensities of the line 4 complex. Since the final state of line 4 has been attributed to the combination $\Gamma_6+\Gamma_7$, a strong 4.5 component is expected for $\mathbf{E}\|\mathbf{F}$, whereas there is little indication that such a component exists at all. In contrast, the weak 4A line appears to give rise to the strong 4.6 component observed for the parallel polarization. In order to understand these anomalies it is necessary to consider the interaction of all the final states giving rise to the line 4 complex.

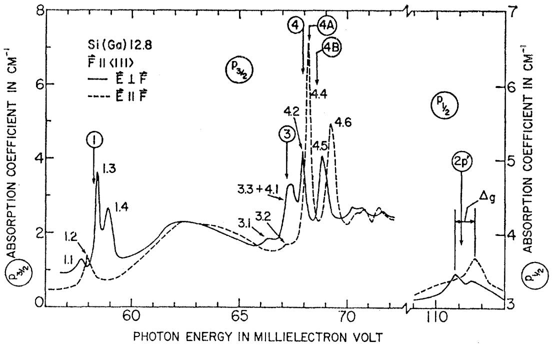

FIG. 26. The effect of a $\langle 111\rangle$ compression on the excitation spectrum of gallium in silicon. Liquid helium was used as coolant; $p(300°\mathrm{K})=2.6\times10^{15}$ cm^{-3}.

As pointed out above, the intensity calculations do predict, in addition to the selection rules deduced from group theory, certain qualitatively clear features which have been observed experimentally. The experimental results reported here have not been compared quantitatively with the theoretical calculations. In order to carry out such a comparison it is essential that the temperature of the sample be determined more precisely. Also, it should be remarked here that the basis functions used in the theoretical calculations are those for a 1*s* ground state and a 2*p* excited state. However, Schechter[46,47] has found it necessary to include *d*-like terms in the ground-state wave function, and *f*-like terms in the excited-state wave function in order to improve his calculation of the energies of the states. The degree to which the inclusion of these terms will affect the calculated relative intensities has not been evaluated.

The calculations of intensities for $\mathbf{F}\|\langle 110\rangle$ are of particular interest since all transitions are allowed by the selection rules. In order to make such a calculation, with C_ϕ/C_ψ as an undetermined parameter, it is necessary to know Δ'/Δ for both the ground state and the excited states. If it is assumed that $\Delta'/\Delta=1$ for the ground state, many striking features of the experimentally observed spectra can be understood using the values of C_ϕ/C_ψ found from the data for $\mathbf{F}\|\langle 111\rangle$ and $\mathbf{F}\|\langle 100\rangle$.

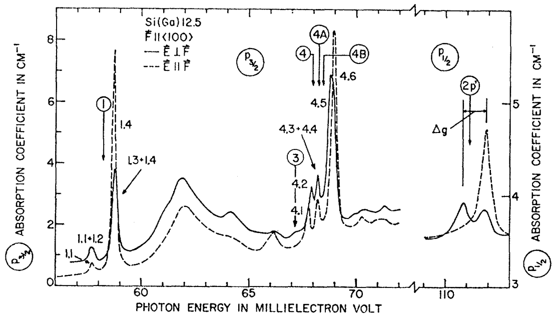

FIG. 27. The effect of a $\langle 100\rangle$ compression on the excitation spectrum of gallium in silicon. Liquid helium was used as coolant; $p(300°\mathrm{K})=2.6\times10^{15}$ cm^{-3}.

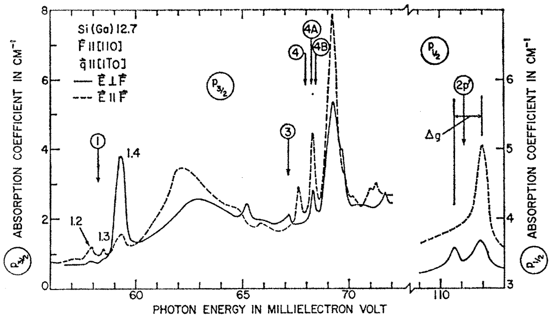

FIG. 28. The effect of a [110] compression on the excitation spectrum of gallium in silicon for q∥[1$\bar{1}$0]. Liquid helium was used as coolant; $p(300°\text{K})=2.6\times10^{15}$ cm^{-3}.

2. *Aluminum*

The effects of uniaxial stress on the spectrum of aluminum impurity are shown in Figs. 22, 23, and 24 for **F**∥⟨111⟩ **F**∥⟨100⟩, and **F**∥[110] **q**∥[1$\bar{1}$0], respectively. The experimentally observed features of lines 1, 2, and $2p'$ are identical in most details to those exhibited by boron. The polarization features of the $2p'$ line indicate that the ground states of aluminum and boron have the same symmetry and stress behavior. Thus the similarity of the spectra implies that for the above transition the excited states also have the same symmetries as in the case of boron. The line-4 complex of aluminum under uniaxial stress is characterized by lack of clear-cut detail, and thus a detailed analysis of the stress dependence of its components has not been attempted. However, the number of strong components observed, their location, and polarization features do not indicate a radically different interpretation from that given for the line 4 complex of boron. For example, for **F**∥⟨111⟩, the two strong parallel components and the three barely resolved perpendicular components occur roughly in the order observed for boron.

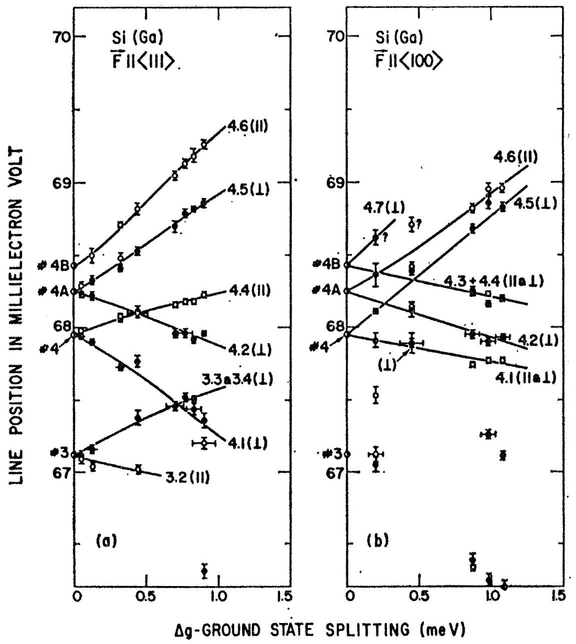

FIG. 29. Positions of the stress-induced components of lines 3, 4, 4A, and 4B of gallium impurity in silicon as a function of ground-state splitting for a compressive force along either ⟨111⟩ or ⟨100⟩. The open circles designate lines observed for **E**∥**F** and the full circles designate lines observed for **E**⊥**F**.

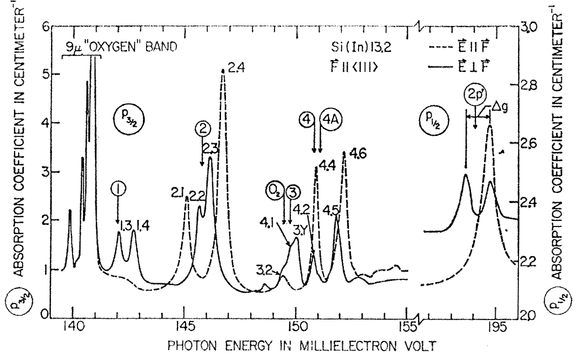

FIG. 30. The effect of a ⟨111⟩ compression on the excitation spectrum of indium in silicon. Liquid helium was used as coolant; $p(300°\text{K})=1.6\times10^{16}$ cm^{-3}.

The effect of a ⟨111⟩ compression on the lines X1 and X3 is shown in Fig. 25. These lines clearly show stress-induced splittings and polarization features. The stress effects appear to rule out the possibility that lines X1 and X3 are localized vibrational modes. For example, no stress dependence of the 9-μ oxygen band is observed even for stresses that produce a 1-meV splitting of the ground state of indium acceptors in silicon (see Sec. IVB 4). The mismatch of the spectra where they overlap is believed to be due to experimental difficulties encountered in this measurement.

3. *Gallium*

In Figs. 26, 27, and 28 are shown the spectra of gallium acceptor with uniaxial compression along ⟨111⟩, ⟨100⟩, and ⟨110⟩, respectively. For lines 1 and $2p'$, the observed stress behavior is similar to that of the corresponding lines of aluminum and boron. It is not surprising that line 2 does not show any distinctive features under stress in view of its anomalous width at zero

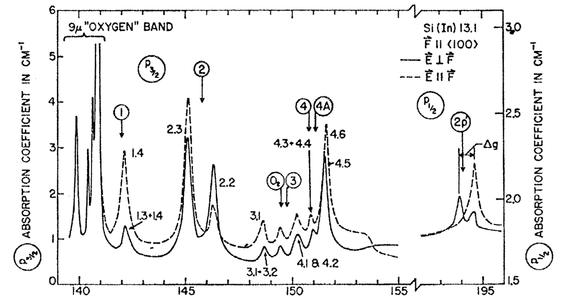

FIG. 31. The effect of a ⟨100⟩ compression on the excitation spectrum of indium in silicon. Liquid helium was used as coolant; $p(300°\text{K})=1.6\times10^{16}$ cm^{-3}.

stress. Thus it is not possible to compare the stress behavior of line 2 of gallium with the corresponding lines of boron and aluminum. However, attention should be drawn to the fact that line 2 of gallium does show some stress dependence in its shape and polarization features. The behavior of line 4 under stress is shown in detail in Fig. 29. There is a clear correspondence between the components of line 4 of gallium and those of boron, and they have been numbered accordingly in both Figs. 21 and 29. The results are consistent with assignments of Γ_7, Γ_6, and Γ_8 for lines 4, 4A, and 4B, respectively. At Δg about 0.45 meV, component 4.2 is seen in the parallel polarization for **F**||⟨100⟩. This is not consistent with the rest of the data nor with the interpretation given. The origin of this behavior is not clear. For **F**||⟨100⟩, it has not been possible to observe the components of line 3 with sufficient reliability to attempt an interpretation of its behavior.

4. Indium

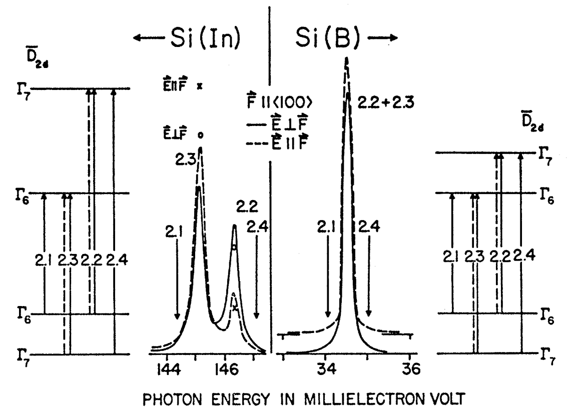

FIG. 33. Comparison of the effect of uniaxial stress on line 2 of boron and indium in silicon for a compressive force along ⟨100⟩, together with the selection rules. The peaks of line 2 of indium impurity at a lower temperature are indicated by X for **E**||**F** and O for **E**⊥**F**. The energy levels are schematic and not to scale. The diagram shows the larger splitting of the excited state of indium compared to that of its ground state. For boron, these splittings are equal, as shown in the diagram.

The effect of uniaxial stress on the spectrum of indium acceptor is shown in Figs. 30, 31, and 32 for **F**||⟨111⟩ **F**||⟨100⟩, and **F**||[110] **q**||[1$\bar{1}$0], respectively. For **F**||⟨111⟩, the polarization patterns of lines 1 and 2 are essentially the same as for boron, except that here the lower-energy components of line 1 are masked by the 9-μ oxygen band. Also, the pattern of line 4 exhibits features that have a clear correspondence with the line 4 complexes of boron and gallium for a given direction of stress. For **F**||[110] **q**||[1$\bar{1}$0], line 1 behaves essentially like line 1 of boron. However, for line 2, the components 2.1 and 2.4 are clearly observed in the parallel polarization while they are very weak in the case of boron. Also, it appears that the components 2.2 and 2.3 are coincident, indicating that the ground state and the excited state have split by the same amount, whereas in the case of the boron, the ground-state splitting is significantly larger than that of the excited state of line 2. The pattern of line 4 in Fig. 32 is distinctly different from the corresponding pattern of the line 4 complex of boron and gallium in that only one strong perpendicular and one strong parallel component is observed. For **F**||⟨100⟩, line 1 appears to behave like line 1 of boron, aluminum, and gallium. As for aluminum and gallium, the splitting of the excited state of line 1 appears to be very small. However, the results for lines 2 and 4 of indium are strikingly different from those observed for the other group-III impurities. For example, line 2 shows two components rather than the component observed for boron and aluminum at the

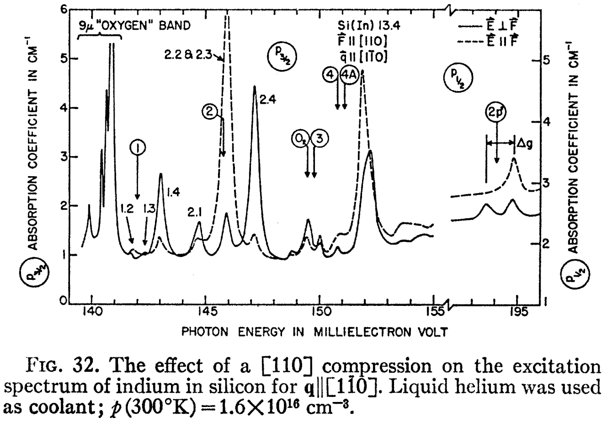

FIG. 32. The effect of a [110] compression on the excitation spectrum of indium in silicon for **q**||[1$\bar{1}$0]. Liquid helium was used as coolant; $p(300°\mathrm{K}) = 1.6\times10^{16}$ cm^{-3}.

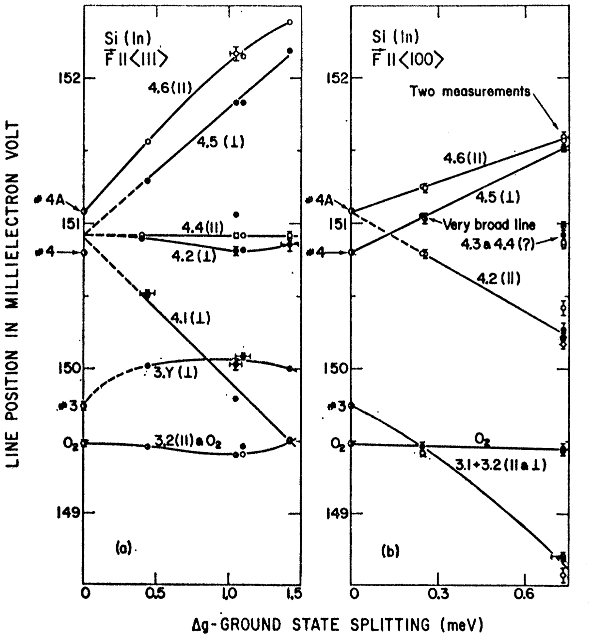

FIG. 34. Positions of the stress-induced components of lines 3, 4, and 4A of indium impurity in silicon as a function of the ground-state splitting for a compressive force along either ⟨111⟩ or ⟨100⟩. The open circles denote lines observed for **E**||**F** and the full circles those observed for **E**⊥**F**.

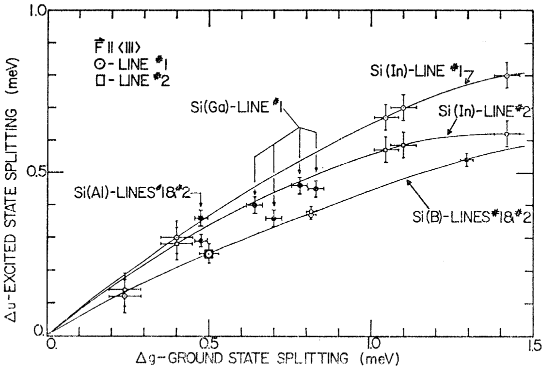

FIG. 35. Excited-state splitting Δu as a function of ground-state splitting Δg for the lines 1 and 2 of the group-III acceptor excitation spectra in silicon under a ⟨111⟩ compression. The curves are drawn through the points for boron and indium impurities. The solid points are for aluminum and gallium impurities.

zero-stress position. Also, the pattern associated with the line-4 complex shows fewer prominent features than observed for boron and gallium.

The behavior of line 2 of boron and indium for **F**∥⟨100⟩ can be understood in terms of Fig. 33. This diagram suggests that line 2 of indium exhibits two stress-induced components because the excited-state splitting is about $2\frac{1}{2}$ times the ground-state splitting, whereas in the case of boron and aluminum it is equal to the ground-state splitting. This interpretation is supported by the observation that as the temperature is lowered, component 2.2 is reduced in intensity while component 2.3 increases in intensity. It is for this reason that the higher-energy component has been labeled 2.2 and the lower 2.3. As can be seen from the figure, this labeling gives a direct correspondence between the transitions observed for indium and boron. The fact that components 2.2 and 2.3 do not coincide in the case of indium impurity for **F**∥⟨100⟩ should permit a comparison of the calculated relative intensities with experiment. In the absence of information regarding the sample temperature, only a qualitative estimate of the ratio C_ϕ/C_ψ consistent with the experimental observations can be obtained from Fig. 3. It is estimated that this ratio is ~ -2, a value similar to that found for boron.

The behavior of line 4 under stress for **F**∥⟨111⟩ and **F**∥⟨100⟩ is shown in Fig. 34. For **F**∥⟨111⟩ there is a clear correspondence of observed components with those seen for boron and gallium, and they have been labeled accordingly. However, it is evident from Figs. 21, 29, and 34 that there are differences in the rates at which the lines split as a function of ground-state splitting for the different impurities. Also, it is evident that the lines drawn through the positions of the appropriate stress-induced components do not extrapolate linearly to the zero-stress positions of either line 3 or line 4. For **F**∥⟨100⟩, the results are not as clear as for boron and gallium and it has not been possible to make symmetry assignments for the excited states. However, on the basis of the pattern of the line 4 complex observed for **F**∥⟨111⟩ it is reasonable to expect that the states which make up the final states of this complex have the same symmetry as in the case of boron and gallium.

5. *Discussion*

Although many similarities in the spectra of the various group-III impurities under stress are apparent in the results presented above, significant differences also emerge. Such differences are brought out particularly clearly when the excited state splitting Δu is plotted against the ground-state splitting, Δg. Such a plot is presented in Fig. 35 for **F**∥⟨111⟩. It is noted in this figure that lines 1 and 2 of boron exhibit the same splitting ratio $\Delta u/\Delta g$, whereas for aluminum and indium this is not the case. Also, it is clear that the excited states of these lines for aluminum, gallium, and indium have a larger splitting relative to that of the ground state than is the case for boron. The ratio $\Delta u/\Delta g$ of lines 1 of aluminum and gallium impurtiy is intermediate to the values of this ratio found for boron and indium. Also, it is clear from Fig. 35 that there is a nonlinear relation between Δu and Δg over the range of stresses employed. This suggests that the linear approximation of the deformation-potential theory for acceptor states is not adequate for the present measurements. Also, the theory does not take into account the species dependence that is evident in the results discussed above. Similar results for **F**∥⟨100⟩ are shown in Fig. 36. The small splitting of the excited state of line 1 for all the impurities investigated is represented by the dashed line at $\Delta u=0$. For line 2, the ratio $\Delta u/\Delta g$ of boron and indium is strikingly different, as has been already

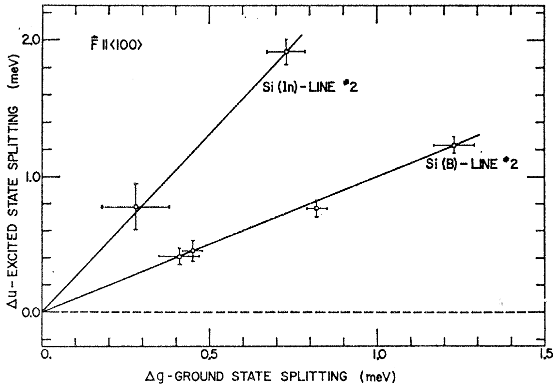

FIG. 36. Excited-state splitting Δu as a function of ground-state splitting Δg for the lines 1 and 2 of the group-III acceptor excitation spectra in silicon under a ⟨100⟩ compression. The dashed horizontal line represents approximately the very small splitting of the excited state of line 1 for all the impurities. For boron, with the exception of the point at $\Delta g=0.84$ meV, the points have been deduced assuming $\Delta u=\Delta g$. The horizontal error bars designate the uncertainty in the determination of Δg from the splitting of the $2p'$ line. The vertical error bars are estimated on the basis of the width of the component 2.2+2.3, which is found to be comparable to the width of the other lines of the spectrum. The point for boron at $\Delta g=0.84$ meV is obtained from a measurement where the component 2.4 was observed.

pointed out. The observed behavior for aluminum impurity is the same as that for boron. It is interesting that, in contrast to the results for $\mathbf{F}\|\langle 111\rangle$, the dependence of Δu on Δg appears to be linear.

V. CONCLUSIONS

In conclusion, the present zero-stress measurements have revealed a wealth of detail not previously observed. Also, comparison of the various experimentally observed features with the existing effective-mass calculations points to a definite need for a renewed theoretical investigation of this problem. In particular, such a theory should be able to account for the chemical species dependence of the excited states. As pointed out in Sec. IVA, the excited states of the various impurities do show a correspondence in spite of these species dependent features. The piezospectroscopic effects support this conclusion as far as the gross features are concerned. The symmetry of the ground state of all the impurities has been established to be Γ_8 of $\bar{T}_d$, in agreement with Schechter's theory.[46,47] It has been deduced that the final states of lines 1, 2, 3, and 5 of boron also belong to Γ_8. The excited state of line 4 of boron behaves in a manner consistent with an assignment of $\Gamma_6+\Gamma_7$, while that of line 4A is consistent with its being a Γ_8 state. For the impurities aluminum, gallium, and indium the symmetries of all these states agree with those of the corresponding states of boron in all the cases where unambiguous results were observed. It has been possible to obtain some insight into the gross features of the relative intensities of the stress-induced components of a given line on the basis of the symmetries of the states participating in the transition. Quantitative differences have been observed in the stress behavior of the corresponding states of the various impurities as well as between states of a given impurity.

ACKNOWLEDGMENTS

The authors wish to thank Professor H. J. Yearian and Miss Louise Roth for orienting the samples used in the present investigation. They are also indebted to S. Balasubramanian for writing a major subroutine that was used in the data analysis.

PHYSICAL REVIEW VOLUME 163, NUMBER 3 15 NOVEMBER 1967

Photoelectric Emission from InAs: Surface Properties and Interband Transitions

T. E. FISCHER,* F. G. ALLEN,† AND G. W. GOBELI‡
Bell Telephone Laboratories, Murray Hill, New Jersey

(Received 13 June 1967)

Photoelectric yield spectra and energy distributions at photon energies between 2.8 and 6.2 eV have been measured for the (110) surface of InAs cleaved in high vacuum and covered with various amounts of cesium. Cleavage produces an inversion layer on the n-type crystal investigated ($N_D=2.5\times10^{15}$ cm^{-3}); on a clean surface the Fermi level coincides with the top of the valence band. The electron affinity and work function of the clean (110) surface are $\chi=4.55\pm0.05$ eV and $\varphi=4.90\pm0.05$ eV, respectively. Deposition of 1/20 monolayer of cesium results in a degenerate n-type surface, which indicates a low density of surface states in the energy gap. Our measurements confirm several important interband transitions in InAs, namely, the Γ_{15v}-Γ_{15c} transition at $h\nu=4.30$ eV, an L_{3v}-L_{3c} transition near $h\nu=6$ eV with a new position of L_{3v} at 1.3 and 1.6 eV below Γ_{15v}, and an X_{5v}-X_{1c} transition at 4.50 eV. We also report two transitions not observed previously. Whatever information can be gained about conservation of the $\mathbf{k}$ vector points to a strong predominance of direct transitions.

I. INTRODUCTION

PHOTOELECTRIC emission has been used for the investigation of surfaces and more extensively for the determination of optical properties and the energy-band structures of solids. In such experiments, one measures the photoelectric yield Y, or total number of electrons emitted per absorbed photon, and the energy distributions dY/dE of the emitted electrons as a function of the photon energy $h\nu$. In surface studies, the interest is concentrated on the determination and interpretation of the photoelectric threshold and the emission properties of neighboring photon energies.[1–8] For the determination of optical properties, on the other hand, one progressively lowers the work function of the

---

[*] Present address: Yale University, New Haven, Connecticut.

[†] Present address: Bellcomm Inc., Washington, D. C.

[‡] Present address: Sandia Corporation, Albuquerque, New Mexico.

[1] E. O. Kane, Phys. Rev. **127**, 131 (1962).

[2] G. W. Gobeli and F. G. Allen, Phys. Rev. **127**, 141 (1962).

[3] F. G. Allen and G. W. Gobeli, Phys. Rev. **127**, 150 (1962).

[4] J. J. Scheer and J. van Laar, Phys. Letters **3**, 246 (1963).

[5] G. W. Gobeli and F. G. Allen, Surface Sci. **2**, 402 (1964).

[6] F. F. Scheer and J. van Laar, Surface Sci. **3**, 189 (1965).

[7] G. W. Gobeli and F. G. Allen, Phys. Rev. **137**, A245 (1965).

[8] T. E. Fischer, Phys. Rev. **142**, 519 (1966).